Dalton Transactions

Accepted Manuscript

ROYAL SOCIETY OF CHEMISTRY

www.rsc.org/dalton

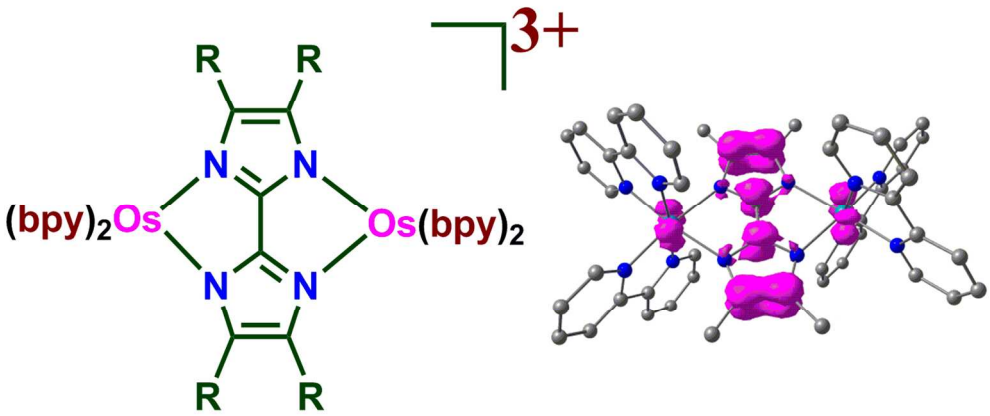

131x54mm (300 x 300 DPI)

Recognition of fractional non-innocent feature of osmium coordinated 2,2′-biimidazole or 2,2′-bis(4,5-dimethylimidazole) and their interactions with anions

Ankita Das,[a] Shaikh M. Mobin,[b] and Goutam Kumar Lahiri*[a]

[a]*Department of Chemistry, Indian Institute of Technology Bombay, Powai, Mumbai-400076, India. E-mail: lahiri@chem.iitb.ac.in*

[b]*Discipline of Chemistry, School of Basic Sciences, Indian Institute of Technology Indore, Indore 452017, India*

The non-innocent feature of osmium coordinated doubly deprotonated 2,2′-biimidazole derivatives in symmetric dimeric complexes leading to mixed electronic structural configuration.

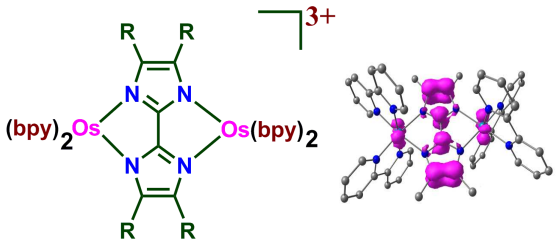

Recognition of fractional non-innocent feature of osmium coordinated 2,2′-biimidazole or 2,2′-bis(4,5-dimethylimidazole) and their interactions with anions

Ankita Das,[a] Shaikh M. Mobin,[b] and Goutam Kumar Lahiri*[a]

[a]*Department of Chemistry, Indian Institute of Technology Bombay, Powai, Mumbai-400076, India. E-mail: lahiri@chem.iitb.ac.in*

[b]*Discipline of Chemistry, School of Basic Sciences, Indian Institute of Technology Indore, Indore 452017, India*

†Electronic supplementary information (ESI) available: X-ray crystallographic file for [**1**]$(ClO_4)_2$, [**3**]$(ClO_4)_2$ and **1** in CIF format, mass spectra (Figs. S1, S2, S9, S11), NMR (Figs. S3, S4, S15-S23), colourimetric results (Fig. S5), UV-vis. plots (Fig. S6, S12), log *K* plots (Figs. S7, S10, S13), pK_a plots (Fig. S8), CV plots (Fig. S14), ORTEP diagram of **1** (Fig. S24), DFT optimised structures (Figs. S25, S26), bond parameters (Tables S1-S2, S16-S17) and DFT data (Tables S3-S15). CCDC nos. 1039323 ([**1**]$(ClO_4)_2$), 1039324 ([**3**]$(ClO_4)_2$), 1039325 (**1**).

Abstract

Mononuclear complexes $[Os^{II}(bpy)_2(H_2L_1)](ClO_4)_2$ [**1**]$(ClO_4)_2$, $[Os^{II}(bpy)_2(H_2L_2)](ClO_4)_2$ [**2**]$(ClO_4)_2$ incorporating two free NH protons at the back face of the coordinated H_2L and deprotonated L^{2-} bridged symmetric dinuclear complexes $[(bpy)_2Os^{II}(\mu\text{-}L_1^{2-})Os^{II}(bpy)_2)](ClO_4)_2$ [**3**]$(ClO_4)_2$, $[(bpy)_2Os^{II}(\mu\text{-}L_2^{2-})Os^{II}(bpy)_2)](ClO_4)_2$ [**4**]$(ClO_4)_2$ (bpy=2,2′-bipyridine, H_2L_1=2,2′-biimidazole and H_2L_2=2,2′-bis(4,5-dimethylimidazole)) have been characterised. Crystal structures of [**1**]$(ClO_4)_2$ and the *meso* (ΔΛ) diastereomeric form of [**3**]$(ClO_4)_2$ have been determined. The crystal structure of [**1**]$(ClO_4)_2$ also reveals the hydrogen bonding interactions between its free acidic NH protons and the oxygen atoms of perchlorate anion in the nearby asymmetric unit. Experimental and DFT/TD-DFT calculations have divulged the non-innocent feature of the doubly deprotonated L^{2-} in $\mathbf{3}^{3+}$or $\mathbf{4}^{3+}$, leading to the resonating formulation of $\{Os^{II}(\mu\text{-}L^{2-})Os^{III}\}\leftrightarrow\{Os^{II}(\mu\text{-}L^{\bullet-})Os^{II}\}$, instead of a simple mixed valent situation $\{Os^{II}(\mu\text{-}L^{2-})Os^{III}\}$. The dinuclear complex $\mathbf{3}^{3+}$or $\mathbf{4}^{3+}$ displays one broad and moderately intense near-IR transition near 1000 nm corresponding to a mixed Os(dπ)/L(π)→Os(dπ)/L(π*) MLLMCT (metal/ligand to ligand/metal charge transfer) transition. Different experimental studies have also established the interaction of $\mathbf{1}^{2+}$ and $\mathbf{2}^{2+}$ with the selective anions.

Introduction

The classical ligand, 2,2′-biimidazole has been utilised since long to fabricate a wide variety of mononuclear and dinuclear metal complexes from the broader perspectives of coordination chemistry.[1] The primary activities are centred around their coordinating behaviour, physico-chemical properties and their potential application towards anion sensing feature via the available free NH protons at the back face of the ligand in the mononuclear systems.[2] The earlier studies have shown that the metal coordinated 2,2′-biimidazole derivatives are essentially redox insensitive, i.e. innocent on electron transfer processes.[1a,d-h,2h,n,3] However, our recent studies with selective ruthenium and analogous osmium complexes of 9-oxidophenalenone,[4] 2,2′-bipyridine-3,3′-diol[5] or 5-(1*H*-benzo[*d*]imidazol-2-yl)-1*H*-imidazole-4-carboxylic acid[6] have revealed the sizeable participation of those ligands in the corresponding MOs leading to the metal-ligand mixed electronic structural configurations in the accessible oxidation processes. This indeed has initiated the present work of developing the less explored[1g] osmium complexes of 2,2′-biimidazole derivatives, mononuclear $\mathbf{1}^{2+}/\mathbf{2}^{2+}$ and dinuclear $\mathbf{3}^{2+}/\mathbf{4}^{2+}$ with the primary objectives of (i) exploring the non-innocent potential

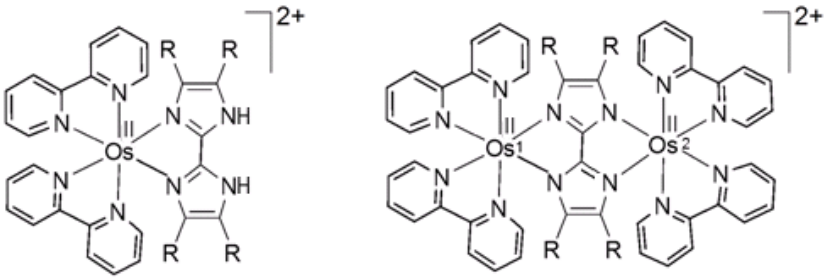

Scheme 1 Representation of complexes.

of osmium coordinated 2,2′-biimidazole derivatives in $\mathbf{1}^{2+}/\mathbf{2}^{2+}$ and/or $\mathbf{3}^{2+}/\mathbf{4}^{2+}$ and (ii) the effectivity of the available free NH groups at the back face of the 2,2′-biimidazole derivatives in the mononuclear $\mathbf{1}^{2+}/\mathbf{2}^{2+}$ towards the recognition of selective anions.

Herein, we report the synthesis, general characterisation, structural and spectro-electrochemical aspects of the mononuclear ($[Os^{II}(bpy)_2(H_2L_1)](ClO_4)_2$ [**1**]$(ClO_4)_2$, $[Os^{II}(bpy)_2(H_2L_2)](ClO_4)_2$ [**2**]$(ClO_4)_2$) and symmetric dinuclear ($[(bpy)_2Os^{II}(\mu\text{-}L_1^{2-})Os^{II}(bpy)_2](ClO_4)_2$ [**3**]$(ClO_4)_2$, $[(bpy)_2Os^{II}(\mu\text{-}L_2^{2-})Os^{II}(bpy)_2](ClO_4)_2$ [**4**]$(ClO_4)_2$) complexes (Scheme 1). The electronic structural aspects of the complexes including the non-innocent potential[4-7] of coordinated H_2L in $\mathbf{1}^n/\mathbf{2}^n$ (n=+2,+3) or L^{2-} in $\mathbf{3}^n/\mathbf{4}^n$ (n=+2,+3,+4) have been investigated by experimental and DFT/TD-DFT studies. Further, the anion sensing features of $\mathbf{1}^{2+}$ and $\mathbf{2}^{2+}$ have been evaluated via a series of experimental and theoretical (DFT) investigations.

Results and discussion

Synthesis, general characterisation and crystal structures

Mononuclear complexes $[Os^{II}(bpy)_2(H_2L)](ClO_4)_2$ [**1**]$(ClO_4)_2$ and [**2**]$(ClO_4)_2$ (bpy=2,2′-bipyridine, H_2L_1=2,2′-biimidazole and H_2L_2=2,2′-bis(4,5-dimethylimidazole)) have been synthesised by the reactions of $Os(bpy)_2Cl_2$ with H_2L_1 and H_2L_2, respectively, in refluxing EtOH-H_2O (1:1) followed by precipitation using saturated aqueous $NaClO_4$ solution. The deprotonated L^{2-} bridged symmetric dinuclear complexes $[(bpy)_2Os^{II}(\mu\text{-}L_1^{2-})Os^{II}(bpy)_2](ClO_4)_2$ ([**3**]$(ClO_4)_2$) and $[(bpy)_2Os^{II}(\mu\text{-}L_2^{2-})Os^{II}(bpy)_2](ClO_4)_2$ ([**4**]$(ClO_4)_2$) have been prepared from the respective mononuclear complexes [**1**]$(ClO_4)_2$ and [**2**]$(ClO_4)_2$ and one mole of $Os(bpy)_2Cl_2$ in refluxing 1:1 EtOH-H_2O in presence of NaOH as a base. The mononuclear and dinuclear complexes have been purified on neutral alumina column using CH_3CN-CH_3OH (1:1) and CH_2Cl_2-CH_3CN (1:1) as eluants, respectively, (Experimental). The exclusive formation of the *meso* ($\Delta\Lambda$) diastereomeric form of $\mathbf{3}^{2+}$ or $\mathbf{4}^{2+}$ has been verified by the preparatory TLC and ^{1}H-NMR experiments.

The diamagnetic and 1:2 conducting [**1**]$(ClO_4)_2$/[**2**]$(ClO_4)_2$ and [**3**]$(ClO_4)_2$/[**4**]$(ClO_4)_2$ exhibit satisfactory microanalytical data (Experimental). The formation of complexes has been authenticated by their mass spectral data in CH_3CN (Figs. S1†, S2† and Experimental). The $\nu(ClO_4)$ vibrations of the complexes in the IR spectra (as KBr disc) appear at around 1100 cm^{-1}, 625 cm^{-1},[7d,8] however, NH vibration of coordinated H_2L in [**1**]$(ClO_4)_2$/[**2**]$(ClO_4)_2$ has not been resolved well due to the appearance of a broad OH vibration around 3400 cm^{-1}. ^{1}H-NMR of $\mathbf{1}^{2+}$ in DMSO-d_6 displays partially overlapping 16 bpy proton resonances and two distinct singlets for 4 CH protons of H_2L_1 corresponding to the full molecule within the chemical shift region δ, 6-9 ppm in addition to one D_2O exchangeable NH signal of H_2L_1 at δ, 13.15 ppm (Fig. S3† and Experimental). On the other hand, ^{1}H-NMR of $\mathbf{2}^{2+}$ in DMSO-d_6

exhibits 8 bpy proton resonances and two singlets for 2 CH_3 groups of H_2L_2 in the chemical shift regions δ, 7-9 ppm and 1-2 ppm, respectively, corresponding to the half molecule due to the internal symmetry (Fig. S3† and Experimental). In comparison to $\mathbf{1}^{2+}$, the D_2O exchangeable NH proton of $\mathbf{2}^{2+}$ appears at slightly up field region of δ, 12 ppm, implying relatively less acidic NH proton of H_2L_2 due to the impact of the electron donating four CH_3 groups as has also been revealed by their pK_a values (see later).[5,9] ^{1}H-NMR of [**3**]$(ClO_4)_2$ or [**4**]$(ClO_4)_2$ in $(CD_3)_2SO$ or CD_3CN, respectively, (Fig. S4† and Experimental) exhibits calculated number of proton resonances corresponding to the half molecule which suggests the exclusive presence of *meso* ($\Delta\Lambda$) diastereomeric form in the solution state.

The crystal structures of representative [**1**]$(ClO_4)_2$ and [**3**]$(ClO_4)_2$ are shown in Fig. 1 and selected crystallographic and bond parameters are given in Table 1 and Tables 2, S1†, respectively. The coordinated planar H_2L_1 is linked to the metal ion in $\mathbf{1}^{2+}$ by its neutral N donors leaving the free NH protons at its back face. The heteroleptic *tris*-chelate situation (bpy and H_2L_1) in $\mathbf{1}^{2+}$ develops a distorted octahedral arrangement with the smaller *trans* and bite angles of 167.9(4)^o-175.0(3)^o) and 75.7(4)^o-79.4(4)^o, respectively.

The crystal structure of [**1**]$(ClO_4)_2$ also reveals hydrogen bonding interactions between its free N-H protons and oxygen atoms of the perchlorate anion in nearby asymmetric unit with N(7)-H(7)...O(7)#1 and N(8)-H(8)...O(6)#1 distances of 2.892 Å and 2.913 Å, respectively[10] (Fig. 1b and Table S2†).

The half-symmetric *meso* ($\Delta\Lambda$) diastereomeric form[11] of planar L_1^{2-} bridged $\mathbf{3}^{2+}$ has been authenticated by its crystal structure (Fig. 1c). The deprotonated symmetric L_1^{2-} bridges the metal ions via $(N,N/N,N)^{2-}$ donors, forming five membered chelates. As in the case of $\mathbf{1}^{2+}$, the heteroleptic *tris*-chelated OsN_6 chromophore in $\mathbf{3}^{2+}$ holds the distorted octahedral

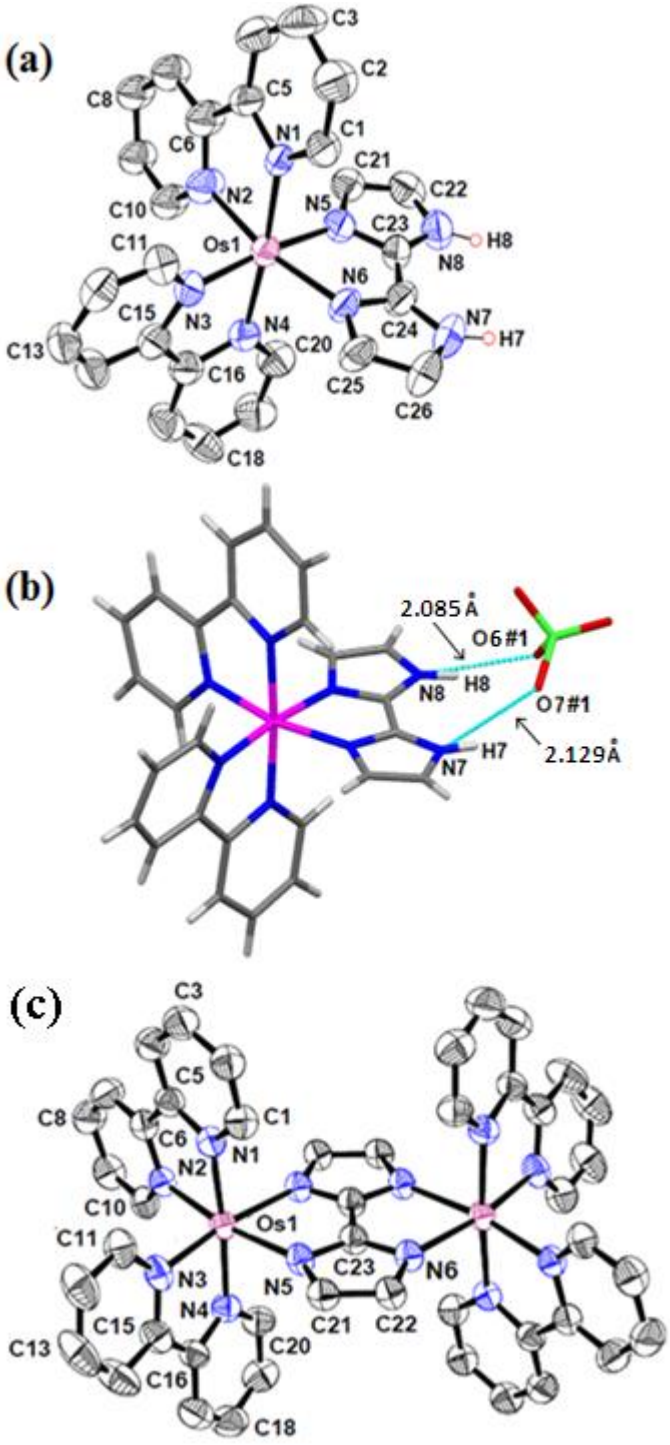

Fig. 1 ORTEP diagram of (a) the dication of [**1**]$(ClO_4)_2$, (b) Perspective view showing the hydrogen bonding interaction between NH protons of $\mathbf{1}^{2+}$ and oxygen atoms of ClO_4^- and (c) ORTEP diagram of the dication of [**3**]$(ClO_4)_2$. Ellipsoids are drawn at 30% probability level and hydrogens (C-H) are omitted for clarity.

Table 1 Selected crystallographic parameters of [**1**]$(ClO_4)_2$ and [**3**]$(ClO_4)_2$

Compound	[**1**]$(ClO_4)_2$	[**3**]$(ClO_4)_2$
Formula	$C_{26}H_{22}N_8O_8Cl_2Os$	$C_{46}H_{36}N_{12}O_8Cl_2Os_2$
M_r	835.61	1336.17
Radiation	CuK_α	CuK_α
Crystal system	Triclinic	Monoclinic
Space group	Pī	I 2/a
a/Å	11.9969(17)	17.1087(10)
b/Å	13.3981(19)	14.5365(6)
c/Å	13.9695(14)	19.9638(11)
α (°)	81.375(10)	90
β (°)	70.669(11)	106.705(6)
γ (°)	85.884(11)	90
V/Å^3	2094.3(5)	4755.5(5)
μ/mm^{-1}	7.320	11.536
Z	2	4
T/K	293(2)	150(2)
ρ_{calcd}/g cm^{-3}	1.325	1.866
F(000)	816	2584
θ range (°)	3.383 to 71.794	3.820 to 71.324
Data/restraints/parameters	7856/3/377	4545/0/316
R1, wR2 ($I>2\sigma(I)$)	0.0880, 0.2363	0.0474, 0.1092
R1, wR2 (all data)	0.1096, 0.2633	0.0751, 0.1299
GOF on F^2	1.017	1.031
Largest diff. peak per hole/e Å^{-3}	1.482/-2.413	1.228/-1.105

geometry as evident by smaller *trans* angles (170.2(3)°-173.9(3)°) and bite angles (78.9(3)°-81.6(2)°).

The average Os^{II}-N(bpy) bond lengths in $\mathbf{1}^{2+}$ and $\mathbf{3}^{2+}$ of 2.025(8) Å and 2.037(7) Å, respectively, are in agreement with the reported Os^{II}-bpy distances in analogous systems.[6a,12]

Table 2 Experimental (X-ray) and DFT calculated bond distances (Å) of [**1**]$(ClO_4)_2$ and [**3**]$(ClO_4)_2$

[**1**]$(ClO_4)_2$			[**3**]$(ClO_4)_2$		
Bond distances (Å)	X-ray	DFT	Bond distances (Å)	X-ray	DFT
Os1-N1	2.037(9)	2.097	Os1-N1	2.045(7)	2.077
Os1-N2	2.040(10)	2.087	Os1-N2	2.040(7)	2.066
Os1-N3	1.988(10)	2.086	Os1-N3	2.021(7)	2.067
Os1-N4	2.037(10)	2.097	Os1-N4	2.044(7)	2.078
Os1-N5	1.995(10)	2.126	Os1-N5	2.141(7)	2.199
Os1-N6	2.082(8)	2.126	Os1-N6#	2.144(6)	2.200
N5-C21	1.419(17)	1.377	N5-C21	1.376(9)	1.384
N5-C23	1.366(15)	1.344	N5-C23	1.323(10)	1.336
N6-C24	1.333(17)	1.344	N6-C23	1.324(10)	1.336
N6-C25	1.401(16)	1.377	N6-C22	1.371(9)	1.384
N7-C24	1.324(16)	1.359	C21-C22	1.367(11)	1.389
N7-C26	1.40(2)	1.378	C23-C23#	1.433(15)	1.409
N8-C22	1.31(2)	1.379			
N8-C23	1.369(17)	1.359			
C21-C22	1.41(2)	1.372			
C23-C24	1.401(18)	1.434			
C25-C26	1.313(19)	1.372			

The shorter Os^{II}-N(bpy) bond length as compared to Os^{II}-N(H_2L_1, 2.038(9) Å in $\mathbf{1}^{2+}$ or L_1^{2-}, 2.142 (7) Å in $\mathbf{3}^{2+}$) is a reflection of stronger $d\pi(Os^{II})\rightarrow\pi^*$(bpy) back bonding interaction.[5a,13] The average Os^{III}-N(H_2L_1) distance of 2.068(2) Å in the other reported derivative $[Os(H_2L_1)_2(OPPh_3)_2]$ $(NO_3)_3$[3b] is close to that in $\mathbf{1}^{2+}$. The two Os centres in $\mathbf{3}^{2+}$ are separated by 5.512 Å. *To the best of our knowledge, [**3**]$(ClO_4)_2$ represents the first structural authentication of L^{2-} bridged diosmium complex.* The average Os^{II}-N(L_1^{2-}) distance of 2.142 (7) Å in $\mathbf{3}^{2+}$ is however matching well with the reported average Ru^{II}-N(L_1^{2-}) distance of 2.141 (6) Å in $[(bpy)_2Ru^{II}((\mu\text{-}L_1^{2-})Ru^{II}(bpy)_2](ClO_4)_2$.[1g]

Electrochemistry, electronic spectra and DFT calculations

The mononuclear complex $\mathbf{1}^{2+}$ or $\mathbf{2}^{2+}$ exhibits one reversible oxidation (Ox1) at E^0_{298}, V(ΔE_p, mV), 0.52(60) or 0.47(60), respectively, and two quasi-reversible successive reversible reductions (Red1 and Red2) in the potential range of -1.6 V to -1.9 V *versus* SCE (Fig. 2, Table 3) with the comproportionation constant, K_c ($RT\ln K_c = nF(\Delta E)$)[14] of 10^5. One-electron nature of the oxidation couple (Ox1) in each case has been confirmed by the constant potential coulometry. The correspondence of the oxidation (Ox1) process in Fig.2 to the

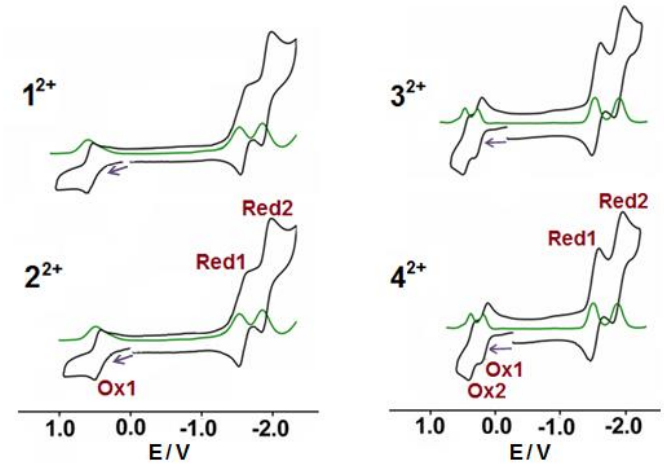

Fig. 2 Cyclic (black) and differential pulse (green) voltammograms in CH_3CN.

dominating Os^{II}/Os^{III} couple[5a,6a] has been substantiated by the relevant MO compositions of $\mathbf{1}^n/\mathbf{2}^n$ (Table 4 and Tables S3-S6†) as well as by the Mulliken spin density plots at the paramagnetic intermediates (Fig. 3, Table 5, Scheme 2). Though spin density calculations predict that Os ion is the sole spin bearing centre in oxidised $\mathbf{1}^{3+}$ (Mulliken spin density, Os:0.953, H_2L_1:0.038, Fig. 3, Table 5), the calculated small contribution of H_2L_2 along with the Os ion in the spin density distribution process in oxidised $\mathbf{2}^{3+}$ (S=1/2) (Mulliken spin density, Os:0.889, H_2L_2:0.114, Fig. 3, Table 5) is however a simple reflection of metal-ligand covalency as has been reported earlier in mononuclear ruthenium[4c-d,15] and osmium[13a,5a] frameworks.

Table 3 Electrochemical data

	$E°_{298}$/V (ΔE_p/mV)[a]				K_c[b]		Reference
Complex	Ox2	Ox1	Red1	Red2	K_{c1}[c]	K_{c2}[d]	
$[Os^{II}(bpy)_2H_2L_1]^{2+}$[e] ($\mathbf{1}^{2+}$)	-	0.52(60)	-1.64(80)	-1.97(120)	-	3.9×10^5	this work
$[Os^{II}(bpy)_2H_2L_2]^{2+}$[e] ($\mathbf{2}^{2+}$)	-	0.47(60)	-1.65(90)	-1.97(120)	-	2.6×10^5	this work
$[Ru^{II}(bpy)_2H_2L_1]^{2+}$[f]	-	1.04(80)	-	-	-	-	1*e*
$[Ru^{II}(bpy)_2H_2L_2]^{2+}$[g]	-	0.77[h]	-	-	-	-	2*n*
$[Ru^{II}(pap)_2H_2L_1]^{2+}$[i]	-	1.70[j]	-	-	-	-	1*g*
$[Os^{II}(pap)_2H_2L_1]^{2+}$[i]	-	1.52[j]	-	-	-	-	1*g*
$[Ru^{III}(acac)_2H_2L_1]^{+}$[e]	1.23(80)	-0.52(90)	-	-	-	-	2*o*
$[(bpy)_2Os(\mu\text{-}L_1)Os(bpy)_2]^{2+}$[e] ($\mathbf{3}^{2+}$)	0.43(60)	0.24(60)	-1.56(130)	-1.92(130)	1.6×10^3	1.2×10^6	this work
$[(bpy)_2Os(\mu\text{-}L_2)Os(bpy)_2]^{2+}$[e] ($\mathbf{4}^{2+}$)	0.41(70)	0.21(60)	-1.55(130)	-1.92(130)	2.4×10^3	1.8×10^6	this work
$[(bpy)_2Ru(\mu\text{-}L_1)Ru(bpy)_2]^{2+}$[k]	1.09(110)	0.75(80)	-	-	5.7×10^5	-	1*f*
$[(pap)_2Ru(\mu\text{-}L_1)Ru(pap)_2]^{2+}$[i]	1.39[h]	1.13[h]	-	-	2.5×10^4	-	1*g*
$[(pap)_2Os(\mu\text{-}L_1)Os(pap)_2]^{2+}$[i]	1.29[h]	1.05[h]	-	-	1.1×10^4	-	1*g*

[a]Potential in V *versus* SCE; peak potential differences ΔE_p/mV (in parentheses). [b]Comproportionation constant from $RT \ln K_c = nF(\Delta E)$. [c]$K_{c1}$ between Ox1 and Ox2. [d]K_{c2} between Red1 and Red2. [e]From cyclic voltammetry in CH_3CN/0.1 M $NEt_4^+ClO_4^-$, scan rate 100 mV s^{-1}. [f]From cyclic voltammetry in CH_3CN/0.1 M $NBu_4^+ClO_4^-$, scan rate 100 mV s^{-1}.[g]From cyclic voltammetry in CH_3CN/0.1 M $NBu_4^+PF_6^-$, scan rate 100 mV s^{-1}. [h]ΔE_p is not reported. [i]From cyclic voltammetry in CH_3CN/0.1 M $NBu_4^+ClO_4^-$, scan rate 50 mV s^{-1}. [j]Irreversible process. [k]From cyclic voltammetry in CH_3CN/0.1 M $NBu_4^+ClO_4^-$, scan rate 100 mV s^{-1}.

The effect of partial mixing of frontier orbitals of H_2L_2 and Os in the MOs has also been reflected in the metal/ligand mixed ($Os(d\pi)/H_2L_2(\pi)\rightarrow bpy(\pi^*)/H_2L_2(\pi^*)$) M/L→L/L charge transfer transition selectively in $\mathbf{2}^{2+}$ (see later). This further highlights that the better mixing of metal-ligand orbitals in the singly occupied MO (SOMO) occurs with the relatively electron rich ligand, H_2L_2 in $\mathbf{2}^{3+}$ *versus* H_2L_1 in $\mathbf{1}^{3+}$ as frequently been noted in the complexes with $\{Ru(acac)_2\}$ metal fragment encompassing electron rich acetylacetonate ($acac^-$).[8,15]

Table 4 DFT calculated selected MO compositions for $\mathbf{1}^n/\mathbf{2}^n$ and $\mathbf{3}^n/\mathbf{4}^n$

Complex	MO	Fragments	% Composition
$\mathbf{1}^{3+}$ (*S*=1/2)	β-LUMO	Os	77
$\mathbf{1}^{2+}$ (*S*=0)	HOMO	Os	74
$\mathbf{2}^{3+}$ (*S*=1/2)	β-LUMO	Os	72
$\mathbf{2}^{2+}$ (*S*=0)	HOMO	Os/H_2L_2	56/34
$\mathbf{3}^{4+}$ (*S*=1)	β-LUMO	Os/bpy	77/15
$\mathbf{3}^{3+}$ (*S*=1/2)	β-HOMO	Os/bpy	77/16
	β-LUMO	Os/ L_1/bpy	59/30/11
$\mathbf{3}^{2+}$ (*S*=0)	HOMO	L_1/bpy/Os	60/30/10
$\mathbf{4}^{4+}$ (*S*=1)	β-LUMO	Os/bpy	77/15
$\mathbf{4}^{3+}$ (*S*=1/2)	β-HOMO	Os/bpy	76/15
	β-LUMO	L_2 /Os/bpy	55/37/08
$\mathbf{4}^{2+}$ (*S*=0)	HOMO	L_2/bpy/Os	95/03/02

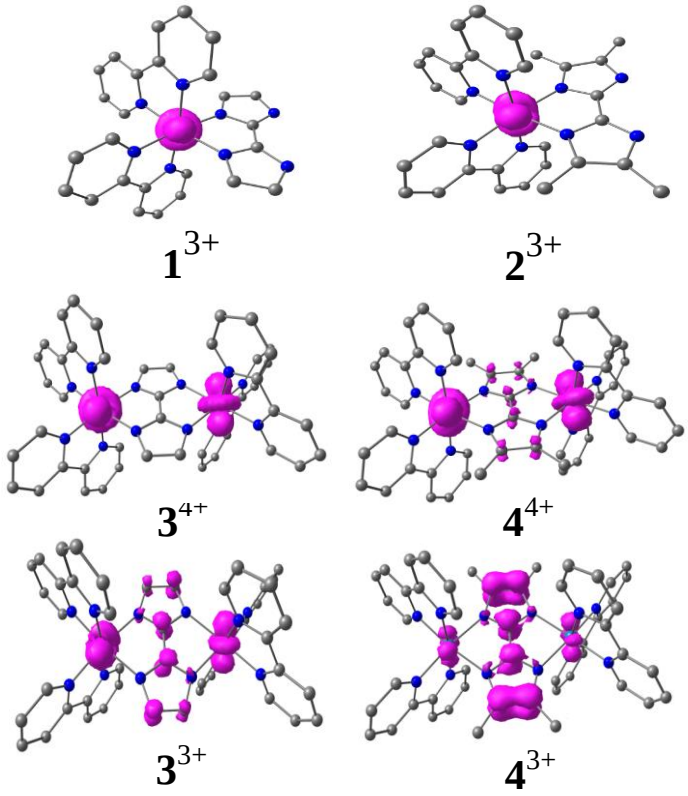

Fig. 3 DFT calculated Mulliken spin density plots of $\mathbf{1}^n/\mathbf{2}^n$ and $\mathbf{3}^n/\mathbf{4}^n$.

Table 5 Mulliken spin density values of $\mathbf{1}^n/\mathbf{2}^n$ (n = +3) and $\mathbf{3}^n/\mathbf{4}^n$ (n = +4, +3) using UB3LYP

Complex	Os1	Os2	H_2L_1/L_1	H_2L_2/L_2	bpy
$\mathbf{1}^{3+}$ (S=1/2)	0.953	-	0.038	-	0.008
$\mathbf{2}^{3+}$ (S=1/2)	0.889	-	-	0.114	-0.004
$\mathbf{3}^{4+}$ (S=1)	0.912	0.912	0.173	-	0.008
$\mathbf{3}^{3+}$ (S=1/2)	0.295	0.290	0.445	-	-0.025
$\mathbf{4}^{4+}$ (S=1)	0.782	0.781	-	0.453	-0.020
$\mathbf{4}^{3+}$ (S=1/2)	0.113	0.116	-	0.788	-0.014

An appreciable negative shift (50 mV) of the oxidation potential (Ox1) has been occurred on moving from $\mathbf{1}^{2+}$ to $\mathbf{2}^{2+}$. The $M^{II}\rightarrow M^{III}$ potentials of $\mathbf{1}^{2+}$ and $\mathbf{2}^{2+}$ along with the reported analogous ruthenium and osmium complexes of H_2L has been placed in Table 3 which reveals the variation of metal oxidation potential primarily based on the differences in π-donor feature of Ru^{II}/Os^{II} [5,6*a*,16] and π-accepting and σ-donating features of bpy (moderately π-accepting)/pap (strongly π- accepting 2-phenylazopyridine) and $acac^-$ (strongly σ-donating acetylacetonate), respectively.[6*b*,17]

The L^{2-} bridged symmetric diosmium(II) complex $\mathbf{3}^{2+}$ or $\mathbf{4}^{2+}$ exhibits stepwise reversible two oxidation (Ox1 and Ox2) and two reduction (Red1 and Red2) processes with the comproportionation constants (K_c) values of ~10^3 and 10^6, respectively (Fig. 2 and Table 3). The one-electron nature of the oxidation processes has been confirmed by the constant potential coulometry. The marginal difference in redox potential of Ox1 or Ox2 between $\mathbf{3}^{2+}$ and $\mathbf{4}^{2+}$ (Table 3) implies insignificant influence of the substituents (R=H *versus* Me, Scheme 1) in the bridge. The appreciably lowered Ox1/Ox2 as well as calculated smaller K_{c1} of $\mathbf{3}^{2+}$ or $\mathbf{4}^{2+}$ (10^3) with respect to the reported analogous L^{2-} bridged Ru and Os complexes (10^4-10^5)[1*e*-*g*,2*n*] (Table 3) suggests considerable effect of π-donor and π-acceptor features of Ru/Os and bpy/pap, respectively.[6*b*,16,17]

Unlike the mononuclear system $\mathbf{1}^{2+}$ or $\mathbf{2}^{2+}$, the MO compositions of $\mathbf{3}^{2+}/\mathbf{4}^{2+}$ and $\mathbf{3}^{3+}/\mathbf{4}^{3+}$ (Table 4 and Tables S7-S8†, S10-S11†) as well as the Mulliken spin densities of paramagnetic intermediates $\mathbf{3}^{3+}$ (Os/L_1: 0.585/0.445) and $\mathbf{4}^{3+}$ (Os/L_2: 0.229/0.788) (Fig. 3, Table 5) collectively suggest the significant involvement of L based orbitals on the first oxidation process (Ox1 in Fig. 2) and it also predict greater contribution of L_2 as compared to L_1 in the singly occupied MOs. This indeed implies that the electronic structural form of the one-electron oxidised $\mathbf{3}^{3+}$ or $\mathbf{4}^{3+}$ can be better described as the resonating form of $\{Os^{II}(\mu\text{-}L^{2-})\ Os^{III}\}\leftrightarrow\{Os^{II}(\mu\text{-}L^{\bullet-})Os^{II}\}$ (Scheme 2), instead of a simple mixed valent situation $\{Os^{II}(\mu\text{-}L^{2-})Os^{III}\}$,[18b,19] as was presumed earlier for the reported L^{2-} bridged analogous diruthenium $[\{(bpy)_2Ru\}_2(\mu\text{-}L^{2-})]^{3+}/[\{(pap)_2Ru\}_2(\mu\text{-}L^{2-})]^{3+}$ and diosmium $[\{(pap)_2Os\}_2(\mu\text{-}L^{2-})]^{3+}$ complexes (Table 3).[1f-g] The appreciable involvement of the bridge in the redox processes due to its non-innocent feature,[11a,20,21] leading to the mixed electronic structural form, has also been recognised recently for the analogous diosmium and diruthenium frameworks of $\{(\mu\text{-}HL^{2-})[Os(bpy)_2]_2\}^n$ (H_3L: 5-(1*H*-benzo[*d*]imidazol-2-yl)-1*H*-imidazole-4-carboxylic acid)[6a] and $\{(\mu\text{-}H_2L)[Ru(AL)_2]_2\}^n$ (AL= $acac^-$ (acetylacetonate), bpy and H_2L=1,4-diimino-9,10-anthraquinone)[22]/$\{(\mu\text{-Nindigo})[Ru(acac)_2]_2\}^n$ (H_2(Nindigo) = indigo-N,N/- diphenylimine),[7a] respectively. The MO compositions of $\mathbf{3}^{3+}/\mathbf{4}^{3+}$ and $\mathbf{3}^{4+}/\mathbf{4}^{4+}$ (Table 4 and Tables S8-S9†, S11-S12†) in conjunction with Mulliken spin density distribution for $\mathbf{3}^{4+}$ (Os/L_1: 1.824/0.173) and $\mathbf{4}^{4+}$ (Os/L_2: 1.563/0.453) (Fig. 3, Table 5), however, reveal a minor contribution of the bridge (L^{2-}) in the doubly oxidised state, leading to the primary electronic structural form of $[(bpy)_2Os^{III}(\mu\text{-}L^{2-})Os^{III}(bpy)_2]^{4+}$ (Scheme 2). Though under the simple metal based successive redox processes, the relatively small K_{c1} value of 10^3 in $\mathbf{3}^{3+}$ or $\mathbf{4}^{3+}$ (Table 3) could be considered as a moderately coupled localised class II mixed valent situation,[6a,18b,23] the extensive mixing of bridge (L) and Os based orbitals particularly in the Ox1 state has however made it inappropriate to evaluate.

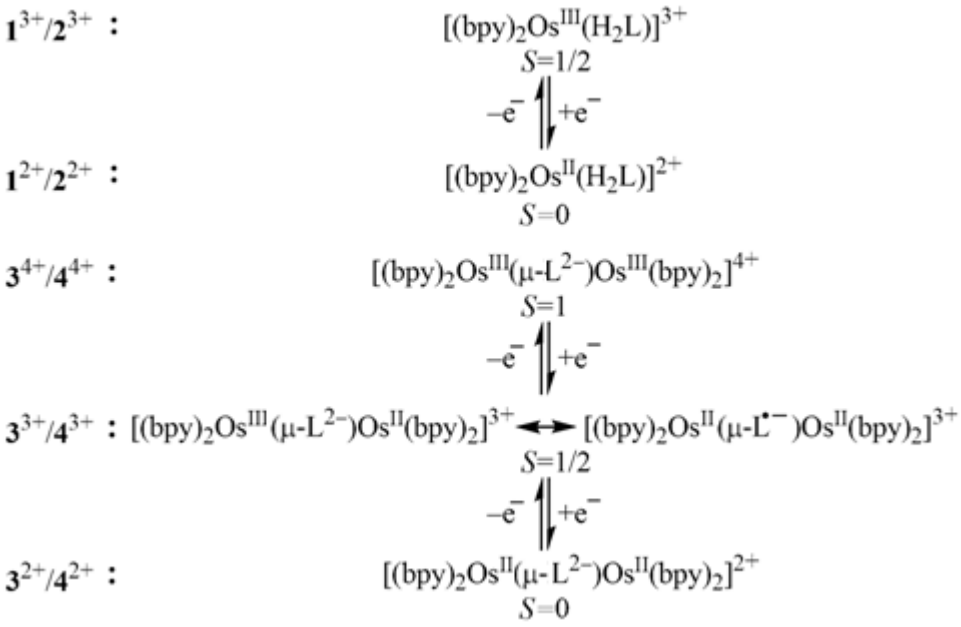

Scheme 2 Electronic structural forms of $\mathbf{1}^n/\mathbf{2}^n$ and $\mathbf{3}^n/\mathbf{4}^n$.

Unfortunately, the electrochemically generated paramagnetic $\mathbf{1}^{3+}/\mathbf{2}^{3+}$ or $\mathbf{3}^{3+}/\mathbf{4}^{3+}$ has failed to display any EPR response at 77 K, presumably due to the rapid relaxation process (~10^{-8} s), being facilitated by the strong spin-orbit coupling effect of Os^{III} (λ, 3000 cm^{-1}) as has also been reported earlier.[18]

The quasi-reversible reduction processes at appreciably high negative potential (> -1.5 V *versus* SCE, Red1 and Red2 in Fig. 2) (Table 3) are found to be unstable at coulometric time scale (5 min.) which indeed has precluded us to check the spectral feature of the electrochemically generated reduced species. The reduction processes are therefore tentatively assigned to be associated with the successive electron uptake processes in the vacant π* orbitals of bpy as has been reported earlier in numerous bpy based analogous complexes.[5*a*,6*a*,24]

The mononuclear complex $\mathbf{1}^{2+}$ or $\mathbf{2}^{2+}$ exhibits close by multiple moderately intense visible bands in addition to intense UV region transitions in CH_3CN (Fig. 4).[5*a*,6*a*,18*b*,25] The transitions are assigned based on the TD-DFT calculations (Table S13†) which however predict significant difference regarding the origin of transitions in $\mathbf{1}^{2+}$ and $\mathbf{2}^{2+}$ in spite of their similar

spectral profile. The multiple visible bands in $\mathbf{1}^{2+}$ essentially correspond to bpy targeted (dπ)Os→π*(bpy) MLCT (metal to ligand charge transfer) and mixed (dπ)Os/(π)bpy→π*(bpy)

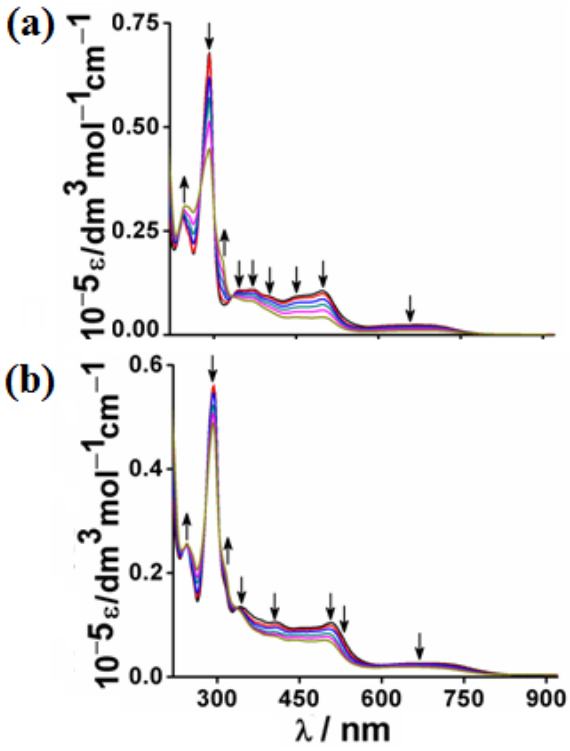

Fig. 4 UV-vis. spectroelectrochemical plots for the conversions of (a) $\mathbf{1}^{2+}\rightarrow\mathbf{1}^{3+}$ and (b) $\mathbf{2}^{2+}\rightarrow\mathbf{2}^{3+}$ (10^{-5} mol dm^{-3}) on sequential additions of $(NH_4)_2Ce(NO_3)_6$ (CAN) (10^{-3} mol dm^{-3}, up to 1eq.) in CH_3CN.

MLLCT (metal/ligand to ligand charge transfer) transitions. On the contrary, the mixing of Os and H_2L_2/bpy based orbitals both in HOMOs and LUMOs in $\mathbf{2}^{2+}$ results in (dπ)Os(II)/(π)H_2L_2→(π*)bpy/(π*)H_2L_2, (dπ)Os(II)/(π)bpy→(π*)bpy/(π*)H_2L_2, (dπ)Os(II)/(π) H_2L_2→(π*)bpy, (π)H_2L_2/(dπ)Os(II)→(π*)bpy based transitions.

The oxidation of $\mathbf{1}^{2+}\rightarrow\mathbf{1}^{3+}$ or $\mathbf{2}^{2+}\rightarrow\mathbf{2}^{3+}$ (chemically or electrochemically) causes slight blue shifting of the visible bands with the reduction in intensity. The bands in $\mathbf{1}^{3+}$ are assigned as (π)bpy or (π)H_2L_1→(dπ)Os based LMCT (ligand to metal charge transfer) transitions. The visible bands in $\mathbf{2}^{3+}$, however, can be better represented as LMLCT or MLLCT transitions where both the ligand orbitals (bpy and H_2L_2) are involved in the HOMOs and LUMOs as in

the native state. The higher energy UV transitions are attributed to intra, inter and mixed ligand (bpy and H_2L_2) based transitions.

The dinuclear complexes $\mathbf{3}^{2+}$ and $\mathbf{4}^{2+}$ display similar spectral profile in CH_3CN with multiple moderately intense close by absorptions in the visible region along with the intense UV transitions.[5,6a,18b,25] The origin of the experimental bands have been assigned by TD-DFT calculations, which predict bpy targeted MLLCT (metal/ligand to ligand charge transfer) transitions in the visible region and inter/intra ligand transitions in the UV region transfer (Fig. 5 and Table S14†).

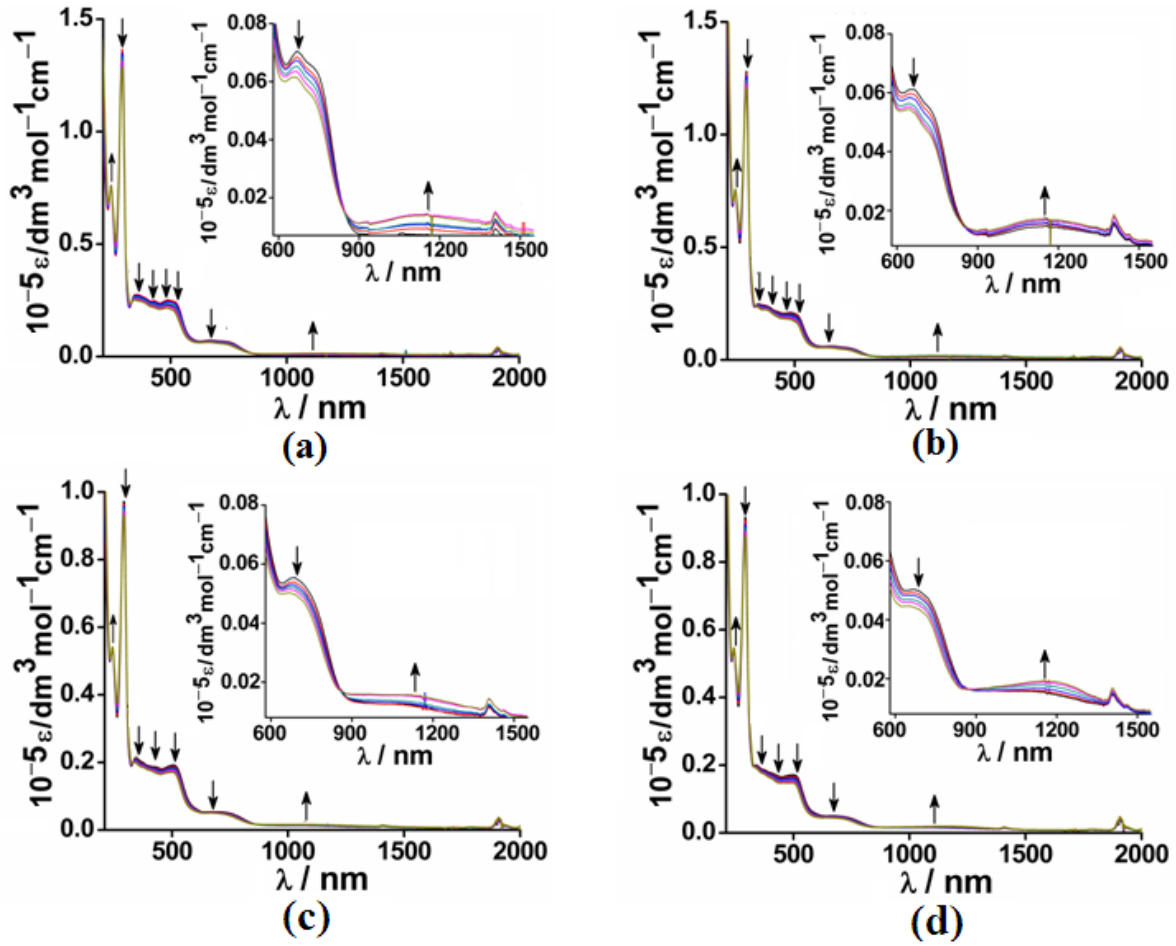

Fig. 5 UV-vis-NIR spectroelectrochemical plots for the conversions of (a) $\mathbf{3}^{2+}\rightarrow\mathbf{3}^{3+}$, (b) $\mathbf{3}^{3+}\rightarrow\mathbf{3}^{4+}$, (c) $\mathbf{4}^{2+}\rightarrow\mathbf{4}^{3+}$ and (d) $\mathbf{4}^{3+}\rightarrow\mathbf{4}^{4+}$ (10^{-5} mol dm^{-3}) on sequential additions of $(NH_4)_2Ce(NO_3)_6$ (CAN) (10^{-3} mol dm^{-3}, up to 2 eq.) in CH_3CN. Inset in each case shows the expanded region, 600 nm-1500 nm.

On oxidation to $\mathbf{3}^{3+}$/$\mathbf{4}^{3+}$, the visible region MLLCT bands undergo slight blue shifting with the reduction in intensity. Furthermore, $\mathbf{3}^{3+}$ or $\mathbf{4}^{3+}$ displays one broad and weak near-IR band at 1152 nm (ε/dm^{3}mol^{-1}cm^{-1}:1400) (TDDFT: 1264 nm) or 1087 nm (ε/dm^{3}mol^{-1}cm^{-1}:1580) (TDDFT: 1319 nm), respectively, corresponding to a mixed Os(dπ)/L(π)→Os(dπ)/L(π*) MLLMCT (metal/ligand to ligand/metal charge transfer) transition (Table S14†). The severe mixing of metal (Os) and bridge (L) based orbitals towards the NIR transition (Table S14†) has precluded its further analysis with special reference to ascertain the mixed valent feature of $\mathbf{3}^{3+}$ or $\mathbf{4}^{3+}$. The intensity of the visible bands reduces to some extent on further oxidation to $\mathbf{3}^{4+}$/$\mathbf{4}^{4+}$, however, the intensity of the near-IR band increases.

Anion recognition features of $\mathbf{1}^{2+}$ and $\mathbf{2}^{2+}$

$\mathbf{1}^{2+}$ or $\mathbf{2}^{2+}$ with two free NH protons at the back face of the coordinated H_2L has been explored with special reference to its potential to function as an effective receptor for selective anions. The anion sensing features of $\mathbf{1}^{2+}$ and $\mathbf{2}^{2+}$ are therefore tested both in acetonitrile and in less explored aqueous medium using series of anions such as tetrabutyl ammonium (TBA) salts of F^-, CN^-, Cl^-, Br^-, I^-, OAc^-, SCN^-, NO_3^-, $H_2PO_4^-$, HSO_4^- via the following techniques.

Colourimetry. The colourimetric technique has been applied for both $\mathbf{1}^{2+}$ or $\mathbf{2}^{2+}$ in CH_3CN to make an initial appraisal in terms of its solution colour in contact with anions. A distinct colour change was observed in case of both $\mathbf{1}^{2+}$ or $\mathbf{2}^{2+}$ on addition of 1 and 4 or 6 equivalents of OAc^-/F^-/CN^- ion, respectively (Fig. S5†), however the colour remains totally unchanged on even excess addition of TBA salts of Cl^-, Br^-, I^-, SCN^-, NO_3^-, HSO_4^- up to 8 equivalents. In addition, the colour of $\mathbf{2}^{2+}$ does not alter with 8 equivalents of $H_2PO_4^-$, however, 1 equivalent of $H_2PO_4^-$ changes the colour of $\mathbf{1}^{2+}$ from brown to pink (Fig. S5†).

The scenario is altogether different in aqueous medium, the colour of $\mathbf{1}^{2+}$ or $\mathbf{2}^{2+}$ changes selectively with 1 or 7 equivalents of CN^- ion, respectively (Fig. S5†).

Colourimetric experiments thus reveal appreciable variation in both $\mathbf{1}^{2+}$ and $\mathbf{2}^{2+}$ based on the solvent medium.

Absorption spectroscopy. The spectral profile of $\mathbf{1}^{2+}$ or $\mathbf{2}^{2+}$ remains same on addition of TBA salts of Cl^-, Br^-, I^-, SCN^-, NO_3^-, HSO_4^- up to 8 equivalents. However, it alters selectively with F^-, CN^-, OAc^- or $H_2PO_4^-$ to different extent (Fig. S6†) in corroboration with the colourimetric experiments (Fig. S5†). The significantly lower basicity (pK_a) of HCl (-7), HBr (-9), HI (-1), HSCN (-2), HNO_3 (-1.3), H_2SO_4 (-2) as compared to HF (3.45), HCN (9.1), HOAc (4.75), H_3PO_4 (2.12)[26] plays a critical role in defining the observed selectivity.

In presence of 1 equivalent of F^- ion, the MLCT band of $\mathbf{1}^{2+}$ at 498 nm is appreciably red-shifted to 530 nm due to the second sphere donor-acceptor interaction. The spectral change is however negligible on addition of 2 equivalents of F^- but 530 nm band gradually shifts to 565 nm with 4 equivalents of F^- and no further spectral change is observed on addition of F^- up to 8 equivalents. The above sequential three-step transformations proceed with two distinct isosbestic points (Fig. 6).

The initial change of 498 nm→530 nm with 1 equivalent of F^- suggests a 1:1 receptor-anion interaction, leading to the monodeprotonation of the coordinated H_2L_1 to HL_1^- in $\mathbf{1}^+$. The binding constant (log K) has therefore been calculated based on eqns (1) and (2),[26,2o] where ΔA represents the change in initial absorbance at 498 nm upon each addition of X^-(X=F^-). $[M(H_2L_n)]^{2+}$ and $[X^-(F^-)]$ correspond to their respective concentrations during the

$$[\{M(H_2L_n)\}]^{2+} + X^- \rightarrow [\{M(H_2L_n)\}]^{2+}\cdot X^-] \rightarrow [\{M(HL_n)\}]^+ + HX \qquad (1)$$

$$K = \frac{[M(H_2L_n)^{2+}\cdot X^-]}{[M(H_2L_n)^{2+}][X^-]}$$

$$\Delta A = \frac{\Delta\varepsilon\,([M(H_2L_n)^{2+}] + 1/K) + (\Delta\varepsilon^2\,([M(H_2L_n)^{2+}] + [X^-] + 1/K)^2 - 4\Delta\varepsilon^2\,[(M(H_2L_n)^{2+}][X^-])^{1/2}}{2} \quad (2)$$

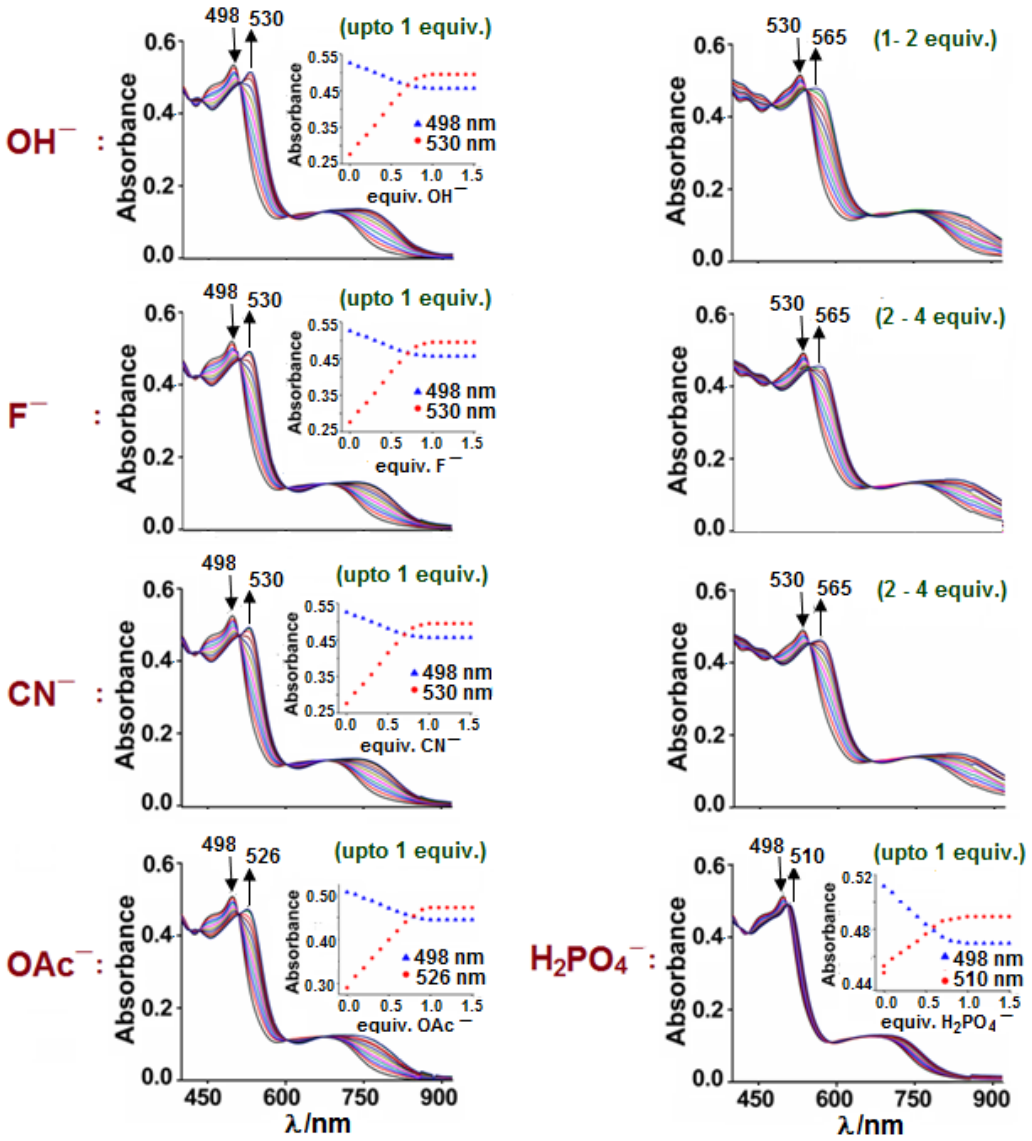

Fig. 6 UV-vis. spectral changes of $\mathbf{1}^{2+}$ (5×10^{-5} mol dm^{-3}) in CH_3CN on gradual additions of OH^-, F^-, CN^-, OAc^- and $H_2PO_4^-$. The inset shows the changes in absorbances at 498 nm, 530 nm for OH^-, F^-, CN^-; 498 nm, 526 nm for OAc^- and 498 nm, 510 nm for $H_2PO_4^-$ as a function of the equivalents of respective anions.

spectrophotometric titrations. The change in molar extinction coefficient ($\Delta\varepsilon$) at each concentration of F^- and binding constant (K) are estimated by the nonlinear curve fitting procedure which results in log K = 6.44 (Fig. S7†). The negligible change in spectral profile on moving from 1 to 2 equivalents of F^- can be attributed to the formation of stable HF_2^- ($HF+F^- \rightarrow HF_2^-$)[27] as has been evidenced by ^{1}H-NMR (see later). The shift in band from 530 nm to 565 nm with the 4 equivalents of F^- corresponds to the doubly deprotonated form of L_1^{2-} in **1** (Scheme 3). The sequential deprotonation of H_2L_1 in $\mathbf{1}^{2+}$ to HL_1^- in $\mathbf{1}^+$ to L_1^{2-} in **1** with 1 and 4 equivalents of F^-, respectively, has been supported by the identical spectral changes of $\mathbf{1}^{2+}$ (498 nm to 530 nm to 565 nm) with 1 and 2 equivalents of stronger base NaOH, respectively (Fig. 6). The specific requirement of more than 2 equivalents of F^- ion (4 equivalents) to deprotonate the second NH proton of H_2L_1 is in agreement with the fact of much higher pK_{a2} (11.5)[28] of $\mathbf{1}^{2+}$ (Fig. S8†). The L_1^{2-} in **1** can be reverted back to the parent H_2L_1 state ($\mathbf{1}^{2+}$) via the intermediate HL_1^- in $\mathbf{1}^+$ by the simple addition of water as a proton source.

The change in spectral profile of $\mathbf{1}^{2+}$ with the CN^- ion in CH_3CN is identical to that of the F^- (Fig. 6). The 1:1 interaction of $\mathbf{1}^{2+}$ and CN^- yields the calculated log K of 6.32 (Fig. S7†).

In contrast to F^- and CN^- ions, the addition of 1 equivalent of OAc^- ion shifts the 498 nm band of $\mathbf{1}^{2+}$ to 526 nm and no further spectral change takes place even with 8 equivalents of OAc^- (Fig. 6). The presence of the strong hydrogen bonding interaction between OAc^- and the receptor could be observed by the formation of $\{\mathbf{1}^+.OAc\}$[6c] association in solution, by an ESI-MS experiment (Fig. S9†), eventually leading to the monodeprotonation of the NH proton upon addition of one equivalent of OAc^-.[29] The 1:1 interaction between the receptor ($\mathbf{1}^{2+}$) and OAc^- results in binding constant value of 6.65 (Fig. S7†). The different interaction mode of OAc^- and $\mathbf{1}^{2+}$ with special reference to F^- or CN^- in spite of relatively high pK_a(aq.)

of HOAc (4.75) (HF(3.45) and HCN(9.1)) emphasises the parallel contributions of both the basicity of the anions and the strength of the hydrogen bonding interaction towards the anion sensing mechanism.

On the other hand, one equivalent of $H_2PO_4^-$ causes only 12 nm red shifting of the MLCT band of $\mathbf{1}^{2+}$ to 510 nm, and it fails to shift the band further on even excess addition up to 8 equivalents (Fig. 6). The 1:1 interaction of $H_2PO_4^-$ and $\mathbf{1}^{2+}$ results in calculated log *K* value of 5.67 (Fig. S7†).

Interestingly, the mode of interaction of complex $\mathbf{2}^{2+}$ with F^- or CN^- in acetonitrile is somewhat different from that of $\mathbf{1}^{2+}$. The MLCT band of $\mathbf{2}^{2+}$ at 508 nm initially moves to 520 nm and then to 545 nm with clean isosbestic points on gradual additions of 0.5 and 1 equivalent of F^- or CN^-, respectively, (Fig. 7), possibly due to the initial hydrogen bonding interaction between the receptor and the anion, which could even be observed spectroscopically, followed by subsequent monodeprotonation to HL_2^- in $\mathbf{2}^+$.

In comparison to $\mathbf{1}^{2+}$, the 1:1 interaction of $\mathbf{2}^{2+}$ and F^- or CN^- results in log *K* values of 5.56 and 5.48, respectively, (Fig. S10†). Unlike $\mathbf{1}^{2+}$, the second deprotonation of $\mathbf{2}^{2+}$ requires 6 equivalents of F^- or CN^- which shifts the 545 nm band further down to 560 nm.

In contrast to $\mathbf{1}^{2+}$ (Fig. 6), the excess $H_2PO_4^-$ (even up to 8 equivalents) fails to alter the spectral pattern of $\mathbf{2}^{2+}$, revealing the impact of marginal difference in acidity of the receptor ($\mathbf{1}^{2+}$ *versus* $\mathbf{2}^{2+}$) particularly towards the interaction with the relatively less basic anion. However, the presence of 1 equivalent of OAc^- results in a stronger hydrogen bonding interaction with the receptor, leading to the formation of $\{\mathbf{2}^+.OAc\}$ association in solution (Fig. S11†), with log *K* value of 5.77 (Fig. S10†), ultimately leading to the monodeprotonated state of HL_2^- in $\mathbf{2}^+$.

The colourimetric features of $\mathbf{1}^{2+}$ and $\mathbf{2}^{2+}$ in aqueous medium (Fig. S5†) have further been explored by the absorption spectroscopy. Though MLCT band of $\mathbf{1}^{2+}$ (498 nm) or $\mathbf{2}^{2+}$ (508

nm) in water is insensitive to F^-, Cl^-, Br^-, I^-, OAc^-, SCN^-, NO_3^-, $H_2PO_4^-$, HSO_4^- , it moves to 526 nm or 530 nm with 1 or 7 equivalents of CN^-, respectively, implying a CN^- selective process (Fig. 8, Fig. S12†).

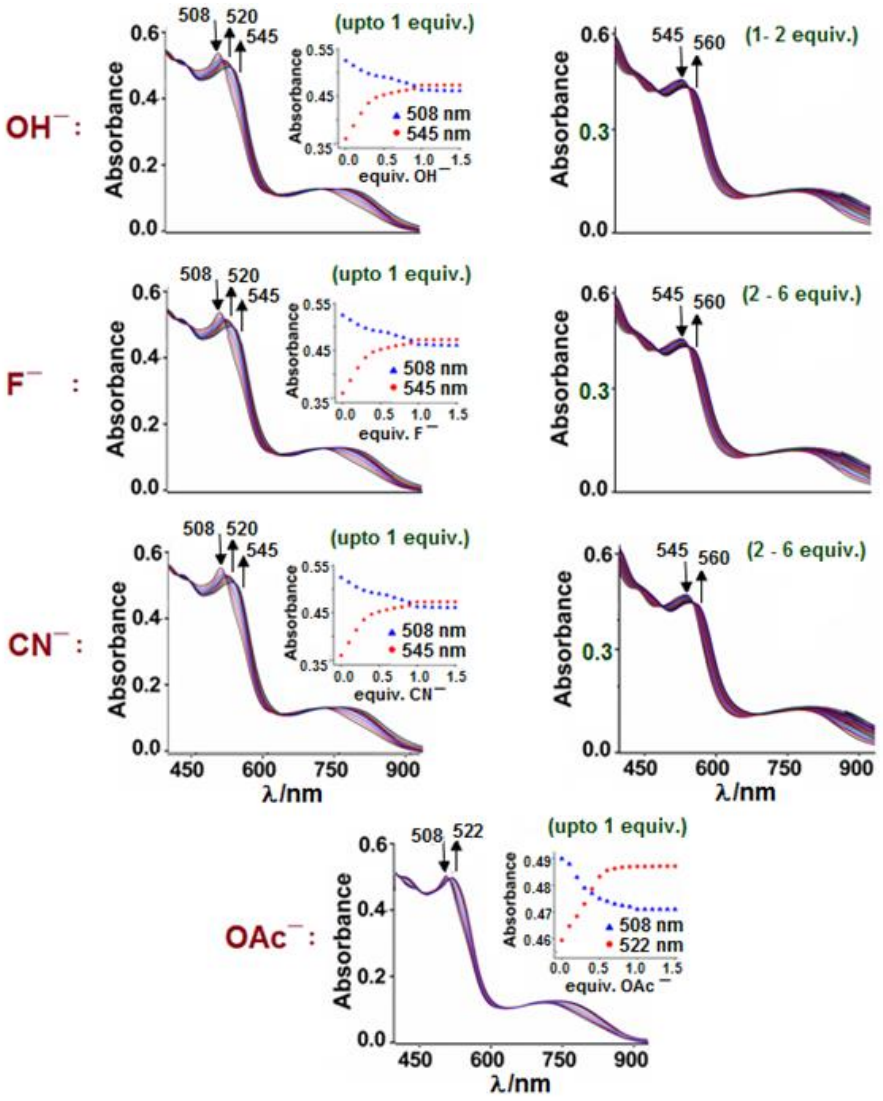

Fig. 7 UV-vis. spectral changes of $\mathbf{2}^{2+}$ ($5x10^{-5}$ mol dm^{-3}) in CH_3CN on gradual additions of $OH^-/F^-/CN^-$ and OAc^-. The inset shows the changes in absorbances at 508 nm, 545 nm for $OH^-/F^-/CN^-$, 508 nm, 522 nm for OAc^- as a function of the equivalents of respective anions.

The partial proton transfer from H_2L of $\mathbf{1}^{2+}$ or $\mathbf{2}^{2+}$ to strongly basic CN^- (pK_a =9.1) through hydrogen bonding interaction increases the electron density over the Os centre, resulting in red-shifts of the absorption band at 498 nm/508 nm to 526 nm/530 nm, respectively, (Fig. 8, Scheme 3).[30,31] The log *K* values for cyanide ion in aqueous medium has been calculated to be 6.54 for $\mathbf{1}^{2+}$ and 4.51 for $\mathbf{2}^{2+}$ (Fig. S13†).

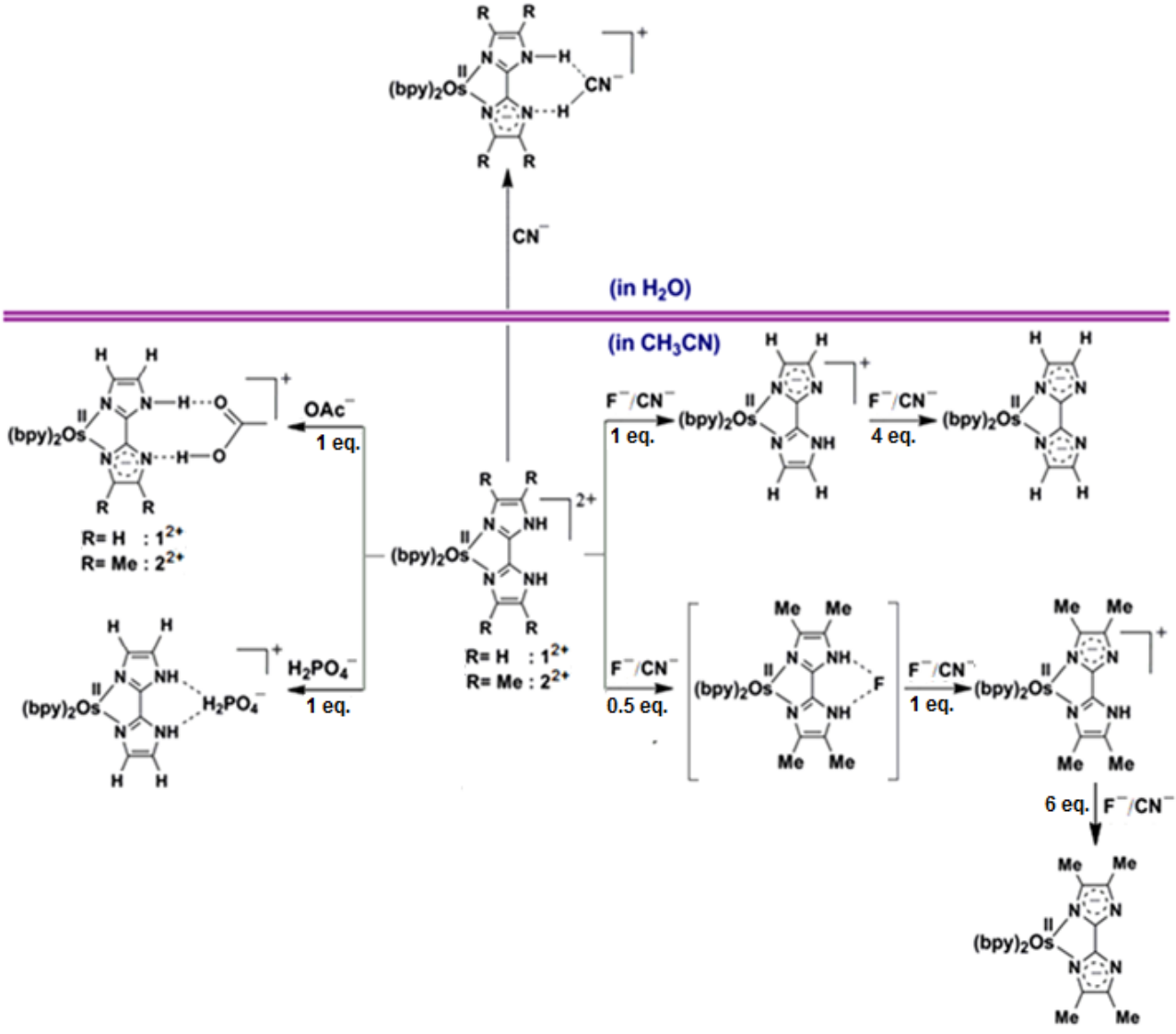

Scheme 3 Schematic representation of interactions of selected anions with $\mathbf{1}^{2+}$ and $\mathbf{2}^{2+}$ in CH_3CN.

The exclusive selectivity of $\mathbf{1}^{2+}$ or $\mathbf{2}^{2+}$ for the CN^- ion in aqueous medium is attributed to its less negative hydration energy (ΔH_{hyd} = -67 kJ/ mol) as compared to that of the F^- ion (ΔH_{hyd} = -505 kJ/mol).[32] The highly solvated F^- ion in water, thus loses its basicity which in turn weakens the feasibility of its interaction with the receptor.[30,33]

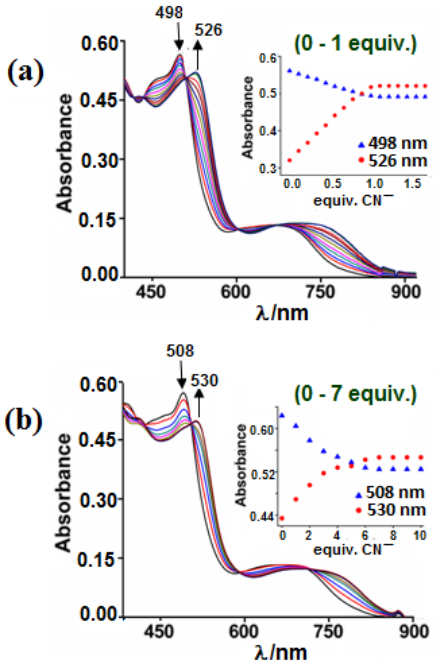

Fig. 8 UV-vis. spectral changes of (a) $\mathbf{1}^{2+}$ and (b) $\mathbf{2}^{2+}$ ($5x10^{-5}$ mol dm^{-3}) in H_2O on gradual additions of up to one and seven equivalents of CN^-, respectively. The insets show the changes in absorbances (a) at 498 nm, 526 nm for $\mathbf{1}^{2+}$ and (b) 508 nm, 530 nm for $\mathbf{2}^{2+}$ as a function of the equivalents of CN^-.

Electrochemistry. The anion recognition feature of $\mathbf{1}^{2+}$ or $\mathbf{2}^{2+}$ has also been evaluated by monitoring the change in redox potential of the oxidation process (Ox1, Fig. 2, Table 3) in acetonitrile as a function of the addition of different anions using cyclic and differential pulse voltammetric techniques. In accordance with the colourimetric and absorption spectroscopic results (preceding sections), the gradual additions of TBA salts of Cl^-, Br^-, I^-, SCN^-, NO_3^-, HSO_4^- fail to make any alteration of the oxidation couple. However, an appreciable variation of oxidation potential has been taken place on addition of 1 equivalent of F^-/CN^-/OAc^-/ $H_2PO_4^-$ for $\mathbf{1}^{2+}$ (Fig. 9) and $\mathbf{2}^{2+}$ (Fig. S14†).

The addition of 1 equivalent of F^- or CN^- to $\mathbf{1}^{2+}$ or $\mathbf{2}^{2+}$ results in a negative shift of the initial oxidation potential, E^0/V at 0.52 V→0.30 V or 0.47 V→0.24 V, respectively, due to the increase in residual electron density on the metal ion by the anion mediated deprotonation of the free NH proton (Scheme 3) of coordinated H_2L. Further addition of F^- or CN^- (> 1 equivalent) in $\mathbf{1}^{2+}$ or $\mathbf{2}^{2+}$ causes the immediate precipitation which indeed has prevented us to follow the second deprotonation process. Almost similar negative shift in oxidation potential

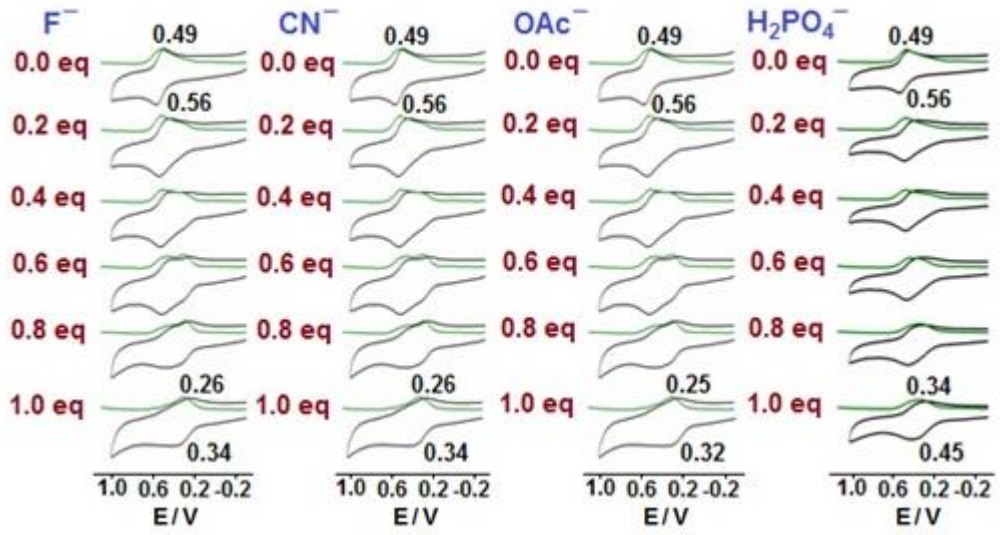

Fig.9 Sequential changes in voltammograms (black) and differential pulse voltammograms (green) (oxidation couple only) of $\mathbf{1}^{2+}$ in CH_3CN (10^{-3} mol dm^{-3}) upon gradual additions of anions.

of $\mathbf{1}^{2+}$ (E^0/V at 0.52 V→0.29 V) or $\mathbf{2}^{2+}$ (E^0/V at 0.47 V→0.23 V) has been recorded with the gradual additions of 1 equivalent of OAc^-. Oxidation potential of $\mathbf{2}^{2+}$ does not alter at all with the addition of 1 equivalent $H_2PO_4^-$ but a relatively small negative shift of potential of $\mathbf{1}^{2+}$ (E^0/V at 0.52 V→0.40 V) is recorded with 1 equivalent $H_2PO_4^-$ in agreement with the colourimetric and absorption spectral events. It thus establishes that $\mathbf{1}^{2+}$ or $\mathbf{2}^{2+}$ can also function as an excellent electrochemical sensor for the selective anions.

NMR spectroscopy. The effectivity of $\mathbf{1}^{2+}$ or $\mathbf{2}^{2+}$ towards the recognition of selective anions has further been rationalised by NMR (^1H, ^{19}F, ^{13}C) technique. In case of both $\mathbf{1}^{2+}$ or

$\mathbf{2}^{2+}$, no such alteration is observed with 8 equivalents of Br^-, Cl^-, I^-, SCN^-, NO_3^-, HSO_4^-. However, the addidition of F^- up to one equivalent results in the disappearance of the NH proton resonance at δ, 13.15 ppm ($\mathbf{1}^{2+}$) or at δ, 12.00 ppm ($\mathbf{2}^{2+}$), due to the initial hydrogen bonding interaction with the anion, leading to the eventual abstraction of the NH proton in the form of HF. Further addition up to 4 or 6 equivalents of F^- in $\mathbf{1}^{2+}$ or $\mathbf{2}^{2+}$, respectively, generates the characteristic triplet of HF_2^- at δ, 16.00 ppm (Figs. S15, S16†, Scheme 3). The effect of removal of the N-H proton(s) of $\mathbf{1}^{2+}$ or $\mathbf{2}^{2+}$ by F^- has also been reflected in the slight

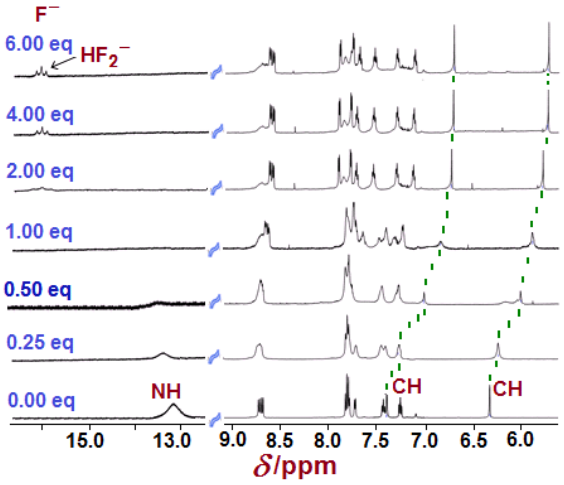

Fig. 10 ^{1}H-NMR titrations of $\mathbf{1}^{2+}$ in DMSO-d_6 with TBA salt of F^- ion (0-6 equivalents).

upfield shift of the singlets involving imidazole ring CH or CH_3 at δ, 7.43 ppm→6.72 ppm/6.34 ppm→5.78 ppm or 2.05 ppm→1.89 ppm/1.04 ppm→1.00 ppm, respectively, as well as slight variation in chemical shifts of the other aromatic protons (Fig. 10 and Fig. S17†). The ^{1}H-NMR spectral features of $\mathbf{1}^{2+}$ or $\mathbf{2}^{2+}$ in presence of other active anions, CN^- and OAc^- (Figs. S18-S21†) also exhibit variations similar to F^- ion. The strong hydrogen bonding interaction between $\mathbf{1}^{2+}$ and $H_2PO_4^{2-}$ has been reflected in the disappearance of NH peak of coordinated H_2L_1 (Fig. S15†).

The ^{19}F-NMR of TBAF in DMSO-d_6 displays two signals at δ, -106.72 ppm and -144.23 ppm corresponding to TBAF and HF_2^-, respectively,[34] where HF_2^- signal originates due to the

effect of moisture in the system. The addition of 0.4 equivalent of $\mathbf{1}^{2+}$ or $\mathbf{2}^{2+}$ to TBAF in DMSO-d_6 leads to the disappearance of the TBAF signal at δ, -106.72 ppm with the simultaneous enhancement of the peak height of HF_2^- signal at -144.23 ppm (Fig. S22†). This indeed justifies the sequence of abstraction of N-H proton of $\mathbf{1}^{2+}$ or $\mathbf{2}^{2+}$ by F^- and reaction of the resultant HF with the excess F^- to yield HF_2^- [35] (Scheme 3).

The upfield shift of ^{13}C-NMR resonance of CN^- in TBACN from δ, 166.21 ppm to 164.02 ppm or 162.39 ppm in presence of 1 equivalent $\mathbf{1}^{2+}$ or $\mathbf{2}^{2+}$ (in DMSO-d_6), respectively, (Fig. S23†) due to the change in electron density on the carbon atom of CN^- extends the further support in favour of deprotonation of the NH proton, via initial hydrogen bonding interaction between the receptor and CN^- [30b,36] (Scheme 3).

Theoretical insights into the anion binding mode of receptors $\mathbf{1}^{2+}$ and $\mathbf{2}^{2+}$. The hydrogen bond mediated deprotonation process between the receptors ($\mathbf{1}^{2+}$ and $\mathbf{2}^{2+}$) and the anions ($F^-/CN^-/OAc^-$) has also been rationalised on the basis of DFT calculations (Scheme 4, Table S15†, Figs.S25, S26†). The calculated longer N8-H8 distance in the optimised **A** (1.554 Å / 1.532 Å) or **B** (1.719 Å / 1.697 Å) or **C** (1.710 Å / 1.690 Å) as compared to that in optimised $\mathbf{1}^{2+}/\mathbf{2}^{2+}$ (1.011 Å / 1.011 Å) and the strong bonding interaction between H8 and F^- (1.005 Å / 1.011 Å in **A**) or CN^- (1.053 Å / 1.059 Å in **B**) or OAc^-(1.017 Å / 1.022 Å in **C**) signify an intermediate situation involving the weakening of the N8-H8 bond with the concomitant formation of the respective H8-X bonds (X= F^-, CN^-, OAc^-). The calculated N8-H8-X angles of 159.5º/160.7º in **A**, 161.6º/163.6º in **B** and 170.4º/169.4º in **C** and D···A distances of 2.52 Å / 2.61 Å in **A**, 2.73 Å / 2.73 Å in **B** and 2.71 Å / 2.70 Å in **C** collectively suggest a hydrogen bond mediated deprotonation process in the presence of anions.[37] The

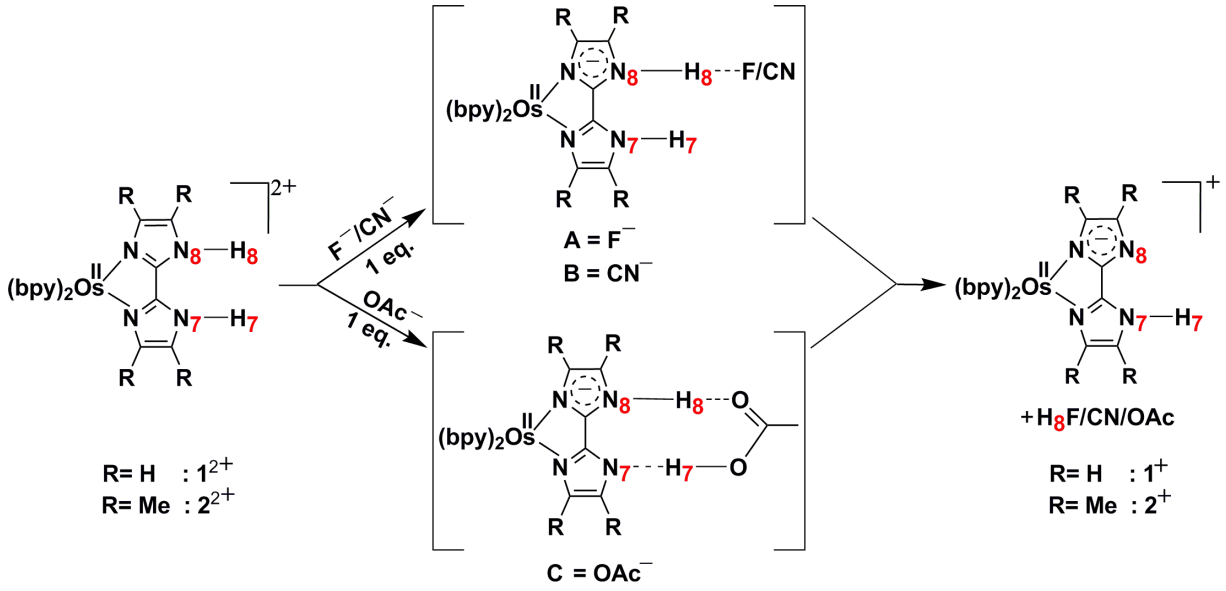

Scheme 4 Hydrogen bond mediated transformations of $\mathbf{1}^{2+}\rightarrow\mathbf{1}^{+}$ or $\mathbf{2}^{2+}\rightarrow\mathbf{2}^{+}$ in presence of X^{-} (X=F/CN/OAc).

slight increase of the natural charge on Os in **A-C** with respect to $\mathbf{1}^{2+}/\mathbf{2}^{2+}$ can be attributed to the change in electronic environment around the metal ion as has also been nicely reflected in the red-shifted MLCT band as well as in the lowering of Os(II)/Os(III) potential.

X-ray crystallography. The selected anion mediated deprotonation of the NH groups of coordinated H_2L in $\mathbf{1}^{2+}$ or $\mathbf{2}^{2+}$ finds direct evidence by the crystal structure determination of **1** (Fig. S24†, Tables S16-S17†), generated via slow evaporation of a mixture of $\mathbf{1}^{2+}$ in presence of excess TBAF in acetonitrile, over a period of weeks. The effect of dianionic L_1^{2-} in **1** has been reflected in the stronger $d\pi(Os^{II})\rightarrow\pi^*(bpy)$ back bonding interaction (average Os^{II}-$N(L_1^{2-})$ distance–average Os^{II}-N(bpy) distance = 0.052 Å) with respect to $\mathbf{1}^{2+}$ incorporating protonated neutral H_2L_1(average Os^{II}-$N(H_2L_1)$distance–average Os^{II}-N(bpy) distance = 0.01 Å).

It is to note that the interaction profile of anions with $\mathbf{1}^{2+}$ is mostly similar to that of the reported ruthenium analogue $[(bpy)_2Ru^{II}(H_2L_1)]^{2+}$ (H_2L_1=2,2′-biimidazole). However, the

present approach of selective use of tetramethyl substituted biimidazole (2,2′-bis(4,5-dimethylimidazole) =H_2L_2) in $\mathbf{2}^{2+}$ could facilitate to even observe the intermediate {$\mathbf{2}^{2+}$.X^-) specie by UV-vis. spectroscopy with 0.5:1 anion-receptor ratio. Furthermore, the receptors $\mathbf{1}^{2+}$ and $\mathbf{2}^{2+}$ could display appreciable variation in terms of their interactions with the anions in both non-aqueous and aqueous media.

Conclusions

In conclusion, the present work demonstrates for the first time the recognition of non-innocent potential of deprotonated L^{2-} in {$Os(bpy)_2$} derived dimeric complexes, leading to the resonating formulation of $[(bpy)_2Os^{II}(\mu\text{-}L^{2-})Os^{III}(bpy)_2]^{3+} \leftrightarrow [(bpy)_2Os^{II}(\mu\text{-}L^{\bullet-})Os^{II}(bpy)_2]^{3+}$ instead of a simple mixed valent situation in $\mathbf{3}^{3+}$ (H_2L_1= 2,2′-biimidazole) or $\mathbf{4}^{3+}$ (H_2L_2 = 2,2′-bis(4,5-dimethylimidazole) (Scheme 2). The detailed studies also reveal that the varying strength of hydrogen bonding interaction with the anions (F^-, CN^-, OAc^-, $H_2PO_4^-$) makes $\mathbf{1}^{2+}$ or $\mathbf{2}^{2+}$ effective anion receptor in non-aqueous medium, while the same receptors are perfectly selective towards the deleterious CN^- ion in water without any interference of the other common anions.

Experimental section

Materials

The starting complex *cis*-$Os^{II}(bpy)_2Cl_2$[38], the ligand 2,2′-Biimidazole[39] (H_2L_1) were prepared according to the reported procedures and the ligand 2,2′-Bis(4,5-dimethylimidazole) (H_2L_2) was purchased from Adrich. Tetrabutylammonium (TBA) salts of F^-, CN^-, Cl^-, Br^-, I^-, HSO_4^-, OAc^-, $H_2PO_4^-$, NO_3^-, SCN^-, OH^- were obtained from Aldrich or Alfa Aesar. Other chemicals and solvents were reagent grade and used as received. For spectroscopic and electrochemical studies HPLC grade solvents were used.

Physical measurements

UV-vis-NIR studies were performed on a Perkin-Elmer Lambda 950 spectrophotometer. Cyclic voltammetric, differential pulse voltammetric and coulometric measurements of the complexes were carried out using a PAR model 273A electrochemistry system. Glassy carbon working electrode, Pt auxiliary electrode and an aqueous saturated calomel reference electrode (SCE) were used in a three-electrode configuration. The supporting electrolyte was $NEt_4^+ClO_4^-$ and the solute concentration was ~10^{-3} M. The half-wave potential E^o_{298} was set equal to 0.5(E_{pa}+ E_{pc}), where E_{pa} and E_{pc} are anodic and cathodic cyclic voltammetric peak potentials, respectively. A platinum wire-gauze working electrode was used in the coulometric experiments. All experiments were carried out under dinitrogen atmosphere. FT-IR spectra were taken on a Nicolet spectrophotometer with samples prepared as KBr pellets. ^{1}H-NMR, ^{19}F-NMR and ^{13}C-NMR spectra were recorded using a Bruker Avance III 500 MHz spectrometer. Trifluoro-toluene was used as an internal standard in DMSO-d_6 for recording ^{19}F-NMR spectra. The elemental analyses were carried out on a Thermoquest (EA 1112) micro analyser. Electrospray mass spectra were recorded on a Bruker's Maxis Impact (282001.00081). The electrical conductivity of the solution was checked by using an Autoranging conductivity meter (Toshcon Industries, India). For spectrophotometric

titrations, in each step 2 μL aliquot of the TBA salt of the respective anions ($5x10^{-3}$ mol dm^{-3}) in CH_3CN or water was added by a micro-syringe in 2 mL CH_3CN or aqueous solution of $\mathbf{1}^{2+}$ or $\mathbf{2}^{2+}$ ($5x10^{-5}$ mol dm^{-3}) using a quartz cuvette with 1 cm path length. For electrochemical titration, 40 μL aliquot of the TBA salt of the respective anions ($5x10^{-2}$ mol dm^{-3}) in acetonitrile was added by a micropipette in each step in 10 mL acetonitrile solution of $\mathbf{1}^{2+}$ or $\mathbf{2}^{2+}$ (10^{-3} mol dm^{-3}).

Cerium ammonium nitrate (CAN) titrations

The acetonitrile solution of CAN (10^{-3} mol dm^{-3}) was gradually added up to 1 and 2 equivalents to the acetonitrile solutions of $\mathbf{1}^{2+}$, $\mathbf{2}^{2+}$ and $\mathbf{3}^{2+}$, $\mathbf{4}^{2+}$ (10^{-5} mol dm^{-3}), respectively, in a cuvette with 1 cm light path length. The absorption spectral changes were monitored after each addition. Each absorption spectrum was plotted on appropriate consideration of the volume change on addition of CAN solution.

Crystallography

Single crystals of [**1**]$(ClO_4)_2$ and [**3**]$(ClO_4)_2$ were grown by slow evaporation of their 1:1 dichloromethane/benzene solutions. Single crystals of **1** were obtained from the acetonitrile solution of $\mathbf{1}^{2+}$ in the presence of excess of TBAF. The X-ray crystal data was collected on a CCD Agilent Technologies (Oxford Diffraction) SUPER NOVA diffractometer. The data was collected by the standard phi-omega scan techniques and was scaled and reduced using CrysAlisPro RED software. The structure was solved by direct methods using SHELXS-97 and refined by full matrix least-squares with SHELXL-2014/7, refining on F^2.[40] All non-hydrogen atoms were refined anisotropically. The remaining hydrogen atoms were placed in geometrically constrained positions and refined with isotropic temperature factors, generally $1.2U_{eq}$ of their parent atoms. Hydrogen atoms were included in the refinement process as per the riding model. The disordered solvent molecules in [**1**]$(ClO_4)_2$ and **1** were SQUEEZED by

PLATON[41] program. The ORTEP diagram of the structures were drawn by using ORTEP 3 program.

Computational details

Full geometry optimisations were carried out by using the density functional theory method at the (R)B3LYP level for $\mathbf{1}^{2+}$, $\mathbf{2}^{2+}$, $\mathbf{3}^{2+}$, $\mathbf{4}^{2+}$, **A**, **B**, **C** and (U)B3LYP level for $\mathbf{1}^{3+}$,$\mathbf{2}^{3+}$, $\mathbf{3}^{4+}$, $\mathbf{3}^{3+}$, $\mathbf{4}^{4+}$, $\mathbf{4}^{3+}$.[42] All elements except osmium were assigned the 6-31G* basis set. The LANL2DZ basis set with effective core potential was employed for the osmium atom.[43] The vibrational frequency calculations were performed to ensure that the optimised geometries represent the local minima and there are only positive eigen values. All calculations were performed with Gaussian09 program package.[44] Vertical electronic excitations based on (R)B3LYP/(U)B3LYP optimised geometries were computed for $\mathbf{1}^n$ (n = +3, +2), $\mathbf{2}^n$ (n = +3, +2), $\mathbf{3}^n$ (n = +4, +3, +2) and $\mathbf{4}^n$ (n = +4, +3, +2) using the time-dependent density functional theory (TD-DFT) formalism[45] in acetonitrile using the conductor-like polarizable continuum model (CPCM).[46] Natural bond orbital analysis was performed using the NBO 3.1 module of Gaussian 09 on optimised geometries. Chemissian *1.7*[47] was used to calculate the fractional contributions of various groups to each molecular orbital. All the calculated structures were visualised with ChemCraft.[48]

Preparation of complexes

Synthesis of $[(bpy)_2Os^{II}(H_2L_1)](ClO_4)_2$, $[1](ClO_4)_2$ and $[(bpy)_2Os^{II}(H_2L_2)](ClO_4)_2$, $[1](ClO_4)_2$. The mixture of the precursor complex *cis*-$Os^{II}(bpy)_2(Cl)_2$ (100 mg, 0.17 mmol) and the ligand 2,2′-Biimidazole (H_2L_1) (27 mg, 0.20 mmol) or 2,2′-Bis(4,5-dimethylimidazole) (H_2L_2) (39 mg, 0.20 mmol) in 30 mL of 1:1 ethanol-water was refluxed under dinitrogen atmosphere for 48 h or 20 h, respectively. The solvent was evaporated to dryness. The dry mass was moistened with a few drops of CH_3CN and saturated aqueous solution of $NaClO_4$ was added. The precipitate thus obtained was filtered off, washed

thoroughly with ice cold water and dried. The crude product was purified by using a neutral alumina column. The brown mononuclear complex [**1**]$(ClO_4)_2$ or [**2**]$(ClO_4)_2$ was eluted by 3:1 acetonitrile-methanol mixture. Evaporation of solvent under reduced pressure yielded the pure complex.

[**1**]$(ClO_4)_2$**:** Yield: 66 mg, 45%. Anal. calcd. for $C_{26}H_{22}N_8Cl_2O_8Os$: C, 37.37; H, 2.65; N, 13.41; Found: C, 36.54; H, 2.58; N, 13.12. Λ_M (Ω^{-1} cm^2 M^{-1}) in acetonitrile at 298 K: 190. ESI-MS(+) in CH_3CN, *m/z*: calcd. for {[**1**]ClO_4}$^+$: 737.16; Found: 737.18. ^{1}H NMR (500 MHz, DMSO-d_6): δ, (ppm, *J*(Hz)): 13.15(s, 2H), 8.70(m, 4H), 7.80(m, 6H), 7.73(d, 2H, 6), 7.46(t, 2H, 6.5), 7.43(s, 2H), 7.28(m, 2H), 6.34(s, 2H).

[**2**]$(ClO_4)_2$**:** Yield: 62 mg, 40%. Anal. calcd. for $C_{30}H_{30}N_8Cl_2O_8Os$: C, 40.41; H, 3.39; N, 12.57; Found: C, 40.23; H, 3.33; N, 12.32. Λ_M (Ω^{-1} cm^2 M^{-1}) in acetonitrile at 298 K: 196. ESI-MS(+) in CH_3CN, *m/z*: calcd. for {[**2**]ClO_4}$^+$: 793.27; Found: 793.04. ^{1}H NMR (500 MHz, DMSO-d_6): δ, (ppm, *J*(Hz)): 12.00 (s, 1H), 8.69 (d, 1H, 8.04), 8.63 (d, 1H, 8.08), 7.79 (d, 1H, 5.6), 7.70 (t, 2H, 7.6), 7.54 (d, 1H, 5.6), 7.47 (t, 1H, 6.6), 7.18 (t, 1H, 6.5), 2.05 (s, 3H), 1.21 (s, 3H).

Synthesis of [(bpy)$_2$Os^{II}(μ-HL$_1^{2-}$)Os^{II}(bpy)$_2$](ClO$_4$)$_2$, ([3](ClO$_4$)$_2$) and [(bpy)$_2$Os^{II}(μ-HL$_2^{2-}$)Os^{II}(bpy)$_2$](ClO$_4$)$_2$, ([4](ClO$_4$)$_2$). The mixture of mononuclear complex [Os^{II}(bpy)$_2$(H_2L_1)]$(ClO_4)_2$ [**1**]$(ClO_4)_2$ (142 mg, 0.17 mmol) or [Os^{II}(bpy)$_2$(H_2L_2)]$(ClO_4)_2$ [**2**]$(ClO_4)_2$ (152 mg, 0.17 mmol), the precursor *cis*-Os(bpy)$_2$Cl$_2$ (100 mg, 0.17 mmol) and NaOH as base (13.6 mg, 0.34 mmol) in 30 mL ethanol-water (1:1) was heated at reflux under dinitrogen atmosphere for 60 h and 48 h, respectively, with simultaneous mechanical stirring. The solution was then evaporated under reduced pressure. The dry mass was moistened with a few drops of CH_3CN and saturated aqueous $NaClO_4$ solution was added to it. The precipitate thus obtained was filtered off, washed thoroughly with ice cold water and dried.

The crude product was purified by using a neutral alumina column, which led to the elution of deep brown coloured complex [**3**]$(ClO_4)_2$ or [**4**]$(ClO_4)_2$ by 1:1 dicholoromethane-acetonitrile mixture. Evaporation of the solvent under reduced pressure yielded the pure complex.

[**3**]$(ClO_4)_2$**:** Yield: 61 mg, 38%. Anal. calcd. for $C_{46}H_{36}N_{12}Cl_2O_8Os_2$: C, 41.35; H, 2.72; N, 12.58; Found: C, 41.53; H, 2.79; N, 12.76. Λ_M (Ω^{-1} cm^2 M^{-1}) in acetonitrile at 298 K: 196. ESI-MS(+) in CH_3CN, *m/z*: calcd. for **3**]$ClO_4\}^+$: 1237.72; Found: 1237.18. ^{1}H NMR (500 MHz, DMSO-d_6): δ, (ppm, *J*(Hz)): 8.63 (d, 2H, 8.2), 8.51 (m, 3H), 8.14 (d, 2H, 6), 7.67 (m, 2H), 7.57 (m, 4H), 7.22 (m, 1H), 7.09 (m, 2H), 5.90 (s, 1H), 5.88 (s, 1H).

[**4**]$(ClO_4)_2$**:** Yield: 55 mg, 35%. Anal. calcd. for $C_{50}H_{44}N_{12}Cl_2O_8Os_2$: C, 43.13; H, 3.19; N, 12.07; Found: C, 43.22; H, 3.13; N, 12.29. Λ_M (Ω^{-1} cm^2 M^{-1}) in acetonitrile at 298 K: 198. ESI-MS(+) in CH_3CN, *m/z*: calcd. for $\{$[**4**]$ClO_4\}^+$: 1293.83; Found: 1293.25. ^{1}H NMR (500 MHz, CD_3CN): δ, (ppm, *J*(Hz)): 8.40 (d, 2H, 7.8), 8.28 (d, 2H, 8.0), 7.84 (m, 2H), 7.68 (m, 4H), 7.54 (m, 2H), 7.17 (m, 2H), 7.00 (m, 2H), 1.26 (s, 6H).

(*CAUTION*! Perchlorate salts are potentially explosive and should be handled with appropriate care).

Acknowledgements

Financial support received from the Department of Science and Technology, Council of Scientific and Industrial Research (Fellowship to AD), New Delhi, India is gratefully acknowledged.

References

1 (*a*) R. Sahai, W. R. Murphy and J. D. Petersen, *Inorg. Chim. Acta*, 1986, **114**, 137; (*b*) M. P. García, A. M. López, M. A. Esteruelas, F. J. Lahoz and L. A. Oro, *J. Chem. Soc., Dalton Trans.*, 1990, 3465; (*c*) T. W. Stringfield, K. V. Somayajula, D. C. Muddiman, J. W. Flora and R. E. Shepherd, *Inorg. Chim. Acta*, 2003, **343**, 317; (*d*) E. V. Dose and L. J. Wilson, *Inorg. Chem*. 1978, **17**, 2660; (*e*) M.-A. Haga, *Inorg. Chim. Acta*, 1983, **75**, 29; (*f*) D. P. Rillema, R. Sahai, P.Matthews, A. K. Edwards, R. J. Shaver and L. Morgan, *Inorg. Chem.*, 1990, 29, 167; (*g*) P. Majumdar, S.-M. Peng and S. Goswami, *J. Chem. Soc., Dalton. Trans*., 1998, 1569; (*h*) P. Majumdar, S. Goswami and S.-M. Peng, *Polyhedron*, 1999, **18**, 2543; (*i*) P. Majumdar, K. K. Kamar, A. Castineiras and S. Goswami, *Chem. Commun*., 2001, 1292; (*j*) B. K. Panda, S. Sengupta and A. Chakravorty, *Eur. J. Inorg. Chem*., 2004, **178**; (*k*) L. Ion, D. Morales, J. Pérez, L. Riera, V. Riera, R. A. Kowenicki and M. McPartlinc, *Chem. Commun*., 2006, **91**; (*l*) M. Barquín, M. J. G. Garmendia and V. Bellido, *Trans. Met. Chem*., 2003, **28**, 356; (*m*) R.-L. Sing and L. Xu, *Inorg. Chim. Acta*, 2006, **359**, 525.

2 (*a*) L. Ion, D. Morales, S. Nieto, J. Perez, L. Riera, V. Riera, D. Miguel, R. A. Kowenicki and M. McPartlin, *Inorg. Chem.*, 2007, **46**, 2846; (*b*) S. Fortin and A. L. Beauchamp, *Inorg. Chem*., 2001, **40**, 105; (*c*) R. Atencio, M. Chacon, T. González, A. Briceño, G. Agrifoglio and A. Sierraalta, *Dalton Trans*., 2004, **505**; (*d*) Y.-R. Zhong, M.-L. Cao, H.-J. Mo and B.-H. Ye, *Cryst. Growth Des.*, 2008, **8**, 2282; (*e*) Y. Cui, H.-J. Mo, J.-C. Chen, Y.-L. Niu, Y.-R. Zhong, K.-C. Zheng and B.-H. Ye, *Inorg. Chem.*, 2007, **46**, 6427; (*f*) A. K. Ghosh, D. Ghoshal, E. Zangrando and N. Ray Chaudhuri, *Polyhedron*, 2007, **26**, 4195; (*g*) S. Fortin, P.-L. Fabre, M. Dartiguenave and A. L. Beauchamp, *J. Chem. Soc., Dalton Trans*., 2001, 3520; (*h*) M. Tadokoro, T. Inoue, S.

Tamaki, K. Fujii, K. Isogai, H. Nakazawa, S. Takeda, K. Isobe, N. Koga, A. Ichimura and K. Nakasuji, *Angew. Chem., Int. Ed.*, 2007, **46**, 5938; (i) R. Atencio, K. Ramírez, J. A. Reyes, T. Gonzalez and P. Silva, *Inorg. Chim. Acta*, 2005, **358**, 520; (j) M. Tadokoro, H. Kanno, T. Kitajima, H. Shimada-Umemoto, N. Nakanishi, K. Isobe and K. Nakasuji, *Proc. Natl. Acad. Sci. U. S. A.*, 2002, **99**, 4950; (*k*) L. M. Gruia, F. D. Rochon and A. L. Beauchamp, *Inorg. Chim. Acta*, 2007, **360**, 1825; (*l*) M. Tadokoro and K. Nakasuji, *Coord. Chem. Rev.*, 2000, **198**, 205; (*m*) Y. Li and P. Yang, *J. Chem. Crystallogr*., 2008, **38**, 529; (*n*) Z.-Z. Li, Y.-L. Niu, H.-Y. Zhou, H.-Y. Chao and B.-H. Ye, *Inorg. Chem*., 2013, **52**, 10087; (*o*) T. Kundu, S. M. Mobin and G. K. Lahiri, *Dalton Trans*., 2010, **39**, 4232.

3 (*a*) N. Sengottuvelan, H.-J. Seo, S. K. Kang, and Y.-I. Kim, *Bull. Korean Chem. Soc*. 2010, **31**, 2309; (*b*) A. Maiboroda, G. Rheinwald and H. Lang, *Eur. J. Inorg. Chem*., 2001, **2263**.

4 (*a*) H. Agarwala, T. M. Scherer, S. M. Mobin and G. K. Lahiri, *Dalton Trans*., 2014, **43**, 3939; (*b*) A. Das, T. K. Ghosh, A. D. Chowdhury, S. M. Mobin and G. K. Lahiri, *Polyhedron*, 2013, **52**, 1130; (*c*) A. Das, T. M. Scherer, P. Mondal, S. M. Mobin, W. Kaim and G. K. Lahiri, *Chem.-Eur. J*., 2012, **18**, 14434; (*d*) A. Das, T. M. Scherer, S. M. Mobin, W. Kaim and G. K. Lahiri, *Inorg. Chem*., 2012, **51**, 4390.

5 (*a*) P. Ghosh, R. Ray, A. Das and G. K. Lahiri, *Inorg. Chem*., 2014, **53**, 10695; (*b*) P. Ghosh, P. Mondal, R. Ray, A. Das, S. Bag, S. M. Mobin and G. K. Lahiri, *Inorg. Chem*., 2014, **53**, 6094.

6 (*a*) A. Das, H. Agarwala, T. Kundu, P. Ghosh, S. M. Mobin and G. K. Lahiri, *Dalton Trans*., 2014, **43**, 13932; (*b*) A. Das, T. Kundu, S. M. Mobin, J. L. Priego, R. Jiménez-Aparicio and G. K. Lahiri, *Dalton Trans.*, 2013, **42**, 13733; (*c*) T. Kundu, A. D.

Chowdhury, D. De, S. M. Mobin, V. G. Puranik, A. Dutta and G. K. Lahiri, *Dalton Trans*., 2012, **41**, 4484.

7 (*a*) P. Mondal, E. Ehret, M. Bubrin, A. Das, S. M. Mobin, W. Kaim and G. K. Lahiri, *Inorg. Chem*., 2013, **52**, 8467; (*b*) D. Das, B. Sarkar, T. K. Mondal, S. M. Mobin, J. Fiedler, W. Kaim and G. K. Lahiri, *Inorg. Chem*., 2011, **50**, 7090; (*c*) S. Ghumaan, S. Mukherjee, S. Kar, D. Roy, S. M. Mobin, R. B. Sunoj and G. K. Lahiri, *Eur. J. Inorg. Chem*., 2006, 4426; (*d*) P. Mondal, S. Plebst, R. Ray, S. M. Mobin, W. Kaim and G. K. Lahiri, *Inorg. Chem*., 2014, **53**, 9348.

8 P. Mondal, H. Agarwala, R. D. Jana, S. Plebst, A. Grupp, F. Ehret, S. M. Mobin, W. Kaim and G. K. Lahiri, *Inorg. Chem.*, 2014, **53**, 7389.

9 H.-J. Mo, Y.-L. Niu, M. Zhang, Z.-P. Qiao and B.-H. Ye, *Dalton Trans.*, 2011, **40**, 8218.

10 (*a*) B. Wu, X. Huang, Y. Xia, X.-J. Yang and C. Janiak, *CrystEngComm*., 2007, **9**, 676; (*b*) H. Hagiwara, S. Hashimoto, N. Matsumoto and S. Iijima, *Inorg. Chem*., 2007, **46**, 3136; (*c*) M. M. Morlok, A. Docrat, K. E. Janak, J. M. Tanski and G. Parkin, *Dalton Trans*., 2004, 3448; (*d*) K. Nishi, S. Arata, N. Matsumoto, S. Iijima, Y. Sunatsuki, H. Ishida and M. Kojima, *Inorg. Chem*., 2010, **49**, 1517; (*e*) A. Sarkar, S. Pal, R. Ghosh, P. K. Dan and B. K. Ghosh, *Indian J. Chem., Sect. A*, 2007, **46A**, 1753; (*f*) G.-H. Lee and H.-T. Wang, *Molecules*, 2007, **12**, 821; (*g*) K. Kaabi, M. El Glaoui, V. Ferretti, M. Zeller and C. B. Nasr, *Acta Crystallogr. Sect. E*, 2011, **67**, o2507.

11 (*a*) D. Kumbhakar, B. Sarkar, S. Maji, S. M. Mobin, J. Fiedler, F. A. Urbanos, R. Jiménez-Aparicio, W. Kaim and G. K. Lahiri, *J. Am. Chem. Soc*., 2008, **130**, 17575;

(*b*) S. Maji, B. Sarkar, S. M. Mobin, J. Fiedler, F. A. Urbanos, R. Jiménez-Aparicio, W. Kaim and G. K. Lahiri, *Inorg. Chem*., 2008, **47**, 5204.

12 S. Ye, B. Sarkar, C. Duboc, J. Fiedler and W. Kaim, *Inorg. Chem.*, 2005, **44**, 2843.

13 (*a*) D. Das, T. M. Scherer, A. Das, T. K. Mondal, S. M. Mobin, J. Fiedler, J. L. Priego, R. Jiménez-Aparicio, W. Kaim and G. K. Lahiri, *Dalton Trans.*, 2012, **41**, 11675; (*b*) G. K. Lahiri, S. Bhattacharya, B. K. Ghosh and A. Chakravorty, *Inorg. Chem*., 1987, **26**, 4324.

14 C. Creutz, *Prog. Inorg. Chem*., 1983, **30**, 1.

15 (*a*) A. Mandal, T. Kundu, F. Ehret, M. Bubrin, S. M. Mobin, W. Kaim and G. K. Lahiri, *Dalton Trans*., 2014, **43**, 2473; (*b*) P. Mondal, R. Ray, A. Das and G. K. Lahiri, *Inorg. Chem.*, 2015, **54**, 3012; (*c*) A. Das, P. Ghosh, S. Plebst, B. Schwederski, S. M. Mobin, W. Kaim and G. K. Lahiri, *Inorg. Chem*., 2015, **54**, 3376.

16 A. Pramanik, N. Bag, D. Ray, G. K. Lahiri and A. Chakravorty, *Inorg. Chem*., 1991, **30**, 410.

17 (*a*) S. Patra, B. Sarkar, S. Maji, J. Fiedler, F. A. Urbanos, R. Jiménez-Aparicio, W. Kaim and G. K. Lahiri, *Chem.-Eur. J*., 2006, **12**, 489; (*b*) S. Kar, B. Sarkar, S. Ghumaan, D. Janardanan, J. V. Slageren, J. Fiedler, V. G. Puranik, R. B. Sunoj, W. Kaim and G. K. Lahiri, *Chem.-Eur. J.*, 2005, **11**, 4901; (*c*) S. Maji, B. Sarkar, S. M. Mobin, J. Fiedler, W. Kaim and G. K. Lahiri, *Dalton Trans*., 2007, 2411.

18 (*a*) J. A. Weil, J. R. Bolton and J. E. Wertz, *Electron Paramagnetic Resonance*, Wiley: New York, 1994, p. 532; (*b*) W. Kaim and B. Sarkar, *Coord. Chem. Rev*., 2013, **257**, 1650.

19 (*a*) A. Das, T. M. Scherer, A. D. Chowdhury, S. M. Mobin, W. Kaim and G. K. Lahiri, *Inorg. Chem*., 2012, **51**, 1675; (*b*) S. Chakraborty, R. H. Laye, P. Munshi, R. L. Paul, M. D. Ward and G. K. Lahiri, *J. Chem. Soc., Dalton Trans*., 2002, 2348; (*c*) B. Sarkar, S. Patra, J. Fiedler, R. B. Sunoj, D. Janardanan, S. M. Mobin, M. Niemeyer, G. K. Lahiri and W. Kaim, *Angew. Chem., Int. Ed*., 2005, **44**, 5655.

22 W. Kaim and G. K. Lahiri, *Angew. Chem., Int. Ed*., 2007, **46**, 1778.

21 B. Sarkar, S. Patra, J. Fiedler, R. B. Sunoj, D. Janardanan, G. K. Lahiri and W. Kaim, *J. Am. Chem. Soc*., 2008, **130**, 3532.

22 A. Mandal, H. Agarwala, R. Ray, S. Plebst, S. M. Mobin, J. L. Priego, R. Jiménez-Aparicio, W. Kaim and G. K. Lahiri, *Inorg. Chem.*, 2014, **53**, 6082.

23 M. B. Robin and P. Day, *Adv. Inorg. Chem. Radiochem*., 1967, **10**, 247.

24 (*a*) S. Ghumaan, B. Sarkar, S. Patra, K. Parimal, J. V. Salgeren, J. Fiedler, W. Kaim and G. K. Lahiri, *Dalton Trans*., 2005, 706; (*b*) S. Roffia, M. Marcaccio, M. C. Paradisi, F. Paoluccil, V. Balzani, J. R. Denti, S. Serroni and M. Campagna, *Inorg. Chem*., 1993, **32**, 3003; (*c*) Y. Sun, N. Ross, S.-B. Zhao, K. Huszarik, W.-L. Jia, R.-Y. Wang, D. Macartney and S. Wang, *J. Am. Chem. Soc*., 2007, **129**, 7510.

25 J. J. Concepcion, M. D. Dattelbaum, T. J. Meyer and R. C. Rocha, *Philos. Trans. R.* Soc. *London*, 2008, **366**, 163.

26 (*a*) Y. Liu, B. -H. Han and Y. -T. Chen, *J. Phys. Chem. B*, 2002, **106**, 4678; (*b*) Y. Liu, B. -H. Han, S. -X. Sun, T. Wada and Y. Inoue, *J. Org. Chem*., 1999, **64**, 1487; (*c*) C. Basu, S. Biswas, A. P. Chattopadhyay, H. Stoeckli-Evans and S. Mukherjee, *Eur. J. Inorg. Chem*., 2008, 4927; (*d*) L. Wang, X.-J. Zhu, W.-Y. Wong, J.-P. Guo, W.-K. Wong and Z.-Y. Li, *Dalton Trans*., 2005, 3235; (*e*) B. Valeur, J. Pouget, J. Bouson,

M. Kaschke and N. P. Ernsting, *J. Phys. Chem*., 1992, **96**, 6545; (*f*) Y. Liu, B. Li, C.-C. You, T. Wada and Y. Inoue, *J. Org. Chem*., 2001, **66**, 225.

27 (*a*) S. O. Kang, D. Powell, V. W. Day and K. Bowman-James, *Angew. Chem., Int. Ed.*, 2006, **45**, 1921; (*b*) I. G. Shenderovich, P. M. Tolstoy, N. S. Golubev, S. N. Smirnov, G. S. Denisov and H.-H. Limbach, *J. Am. Chem. Soc*., 2003, **125**, 11710.

28 F. Holmes, K. M. Jones and E. G. Torrible, *J. Chem. Soc*., 1961, 4790.

29 J. Yin and R. L. Elsenbaumer, *Inorg. Chem*., 2007, **46**, 6891.

30 (*a*) S. Khatua, D. Samanta, J. W. Bats and M. Schmittel, *Inorg. Chem*., 2012, **51**, 7075; (*b*) H.-J. Mo, Y. Shen and B.-H. Ye, *Inorg. Chem*., 2012, **51**, 7174; (*c*) N. Kumari, S. Jha and S. Bhattacharya, *J. Org. Chem*., 2011, **76**, 8215; (*d*) C. B. Black, B. Andrioletti, A. C. Try, C. Ruiperez and J. L. Sessler, *J. Am. Chem. Soc*., 1999, **121**, 10438.

31 (*a*) R. M. F. Batista, V. Oliveira, S. P. G. Costa, C. Lodeiro and M. M. M. Raposo, *Supramolecular Chemistry*, 2014, **26**, 71; (*b*) Z. Xu, X. Chen, H. N. Kim and J. Yoon, *Chem. Soc. Rev*., 2010, **39**, 127; (*c*) R. Manivannan, A. Satheshkumar and K. P. Elango, *New J. Chem*., 2013, **37**, 3152.

32 (*a*) S. Saha, A. Ghosh, P. Mahato, S. Mishra, S. K. Mishra, E. Suresh, S. Das and A. Das, *Org. Lett*., 2010, **12**, 3406; (*b*) C. E. Housecroft and A. G. Sharpe, *Inorganic Chemistry*, Pearson Education Ltd., 3rd Ed., *Harlow*, 2008, p. 537-591.

33 (*a*) R. S. Sathish, U. Sujith, G. N. Rao and C. Janardhana, *Spectrochim. Acta Part A*, 2006, **65**, 565; (*b*) M. Boiocchi, L. Del Boca, D. E. Gomez, L. Fabbrizzi, M. Licchelli and E. Monzani, *J. Am. Chem. Soc*., 2004, **126**, 16507.

34 (*a*) C.-I. Lin, S. Selvi, J.-M. Fang, P.-T. Chou, C.-H. Lai and Y.-M. Cheng, *J. Org. Chem*., 2007, **72**, 3537; (*b*) Z. Xu, N. J. Singh, S. K. Kim, D. R. Spring, K. S. Kim and J. Yoon, *Chem.-Eur. J*., 2011, **17**, 1163.

35 (*a*) D. F. Shriver and P. W. Atkins, *Inorganic Chemistry*, Oxford University Press, 3rd Ed. 1999; (*b*) T. D. B. Morgan, G. Stedman and P. A. E. Whincup, *J. Chem. Soc*., 1965, 4813; (*c*) T. I. Crowell and M. G. Hankins, *J. Phys. Chem*., 1969, **73**, 1380; (*d*) Y. Cui, Y.-L. Niu, M.-L. Cao, K. Wang, H.-J. Mo, Y.-R. Zhong and B.-H. Ye, *Inorg. Chem.*, 2008, **47**, 5616.

36 T. Steiner, *Angew. Chem., Int. Ed*., 2002, **41**, 48.

37 (*a*) T. Ghosh and B. G. Maiya, *J. Phys. Chem. A*, 2004, **108**, 11249; (*b*) M. Sarkar, R. Yellampalli, B. Bhattacharya, R. K. Kanaparthi and A. Samanta, *J. Chem. Sci*., 2007, **119**, 91; (*c*) D. W. Kim, J. Kim, J. Hwang, J. K. Park and J. S. Kim, *Bull. Korean Chem. Soc*., 2012, **33**, 1159.

38 P. A. Lay, M. Sargeson and H. Taube, *Inorg. Synth*., 1986, **24**, 291.

39 J.-C. Xiao and J. M. Shreeve, *J. Org. Chem*., 2005, **70**, 3072.

40 (*a*) G. M. Sheldrick, *Acta Crystallogr. Sect. A*, 2008, **A64**, 112; (*b*) *Program for Crystal Structure Solution and Refinement*, University of Goettingen: Goettingen, Germany, 1997.

41 P. V. D. Sluis and A. L. Spek, *Acta Crystallogr., Sect. A*, 1990, **46**, 194.

42 C. Lee, W. Yang and R. G. Parr, *Phys. Rev. B*, 1988, **37**, 785.

43 (*a*) D. Andrae, U. Haeussermann, M. Dolg, H. Stoll and H. Preuss, *Theor. Chim. Acta*, 1990, **77**, 123; (*b*) P. Fuentealba, H. Preuss, H. Stoll and L. V. Szentpaly, *Chem. Phys. Lett.*, 1989, **89**, 418.

44 M. J. Frisch, G. W. Trucks, H. B. Schlegel, G. E. Scuseria, M. A. Robb, J. R. Cheeseman, G. Scalmani, V. Barone, B. Mennucci, G. A. Petersson, H. Nakatsuji, M. Caricato, X. Li, H. P. Hratchian, A. F. Izmaylov, J. Bloino, G. Zheng, J. L. Sonnenberg, M. Hada, M. Ehara, K. Toyota, R. Fukuda, J. Hasegawa, M. Ishida, T. Nakajima, Y. Honda, O. Kitao, H. Nakai, T. Vreven, J. A. Montgomery, Jr. J. E. Peralta, F. Ogliaro, M. Bearpark, J. J. Heyd, E. Brothers, K. N. Kudin, V. N. Staroverov, R. Kobayashi, J. Normand, K. Raghavachari, A. Rendell, J. C. Burant, S. S. Iyengar, J. Tomasi, M. Cossi, N. Rega, J. M. Millam, M. Klene, J. E. Knox, J. B. Cross, V. Bakken, C. Adamo, J. Jaramillo, R. Gomperts, R. E. Stratmann, O. Yazyev, A. J. Austin, R. Cammi, C. Pomelli, J. W. Ochterski, R. L. Martin, K. Morokuma, V. G. Zakrzewski, G. A. Voth, P. Salvador, J. J. Dannenberg, S. Dapprich, A. D. Daniels, O. Farkas, J. B. Foresman, J. V. Ortiz, J. Cioslowski and D. J. Fox, Gaussian 09 (Revision A.02): Gaussian, Inc.: Wallingford CT 2009.

45 (*a*) R. Bauernschmitt and R. Ahlrichs, *Chem. Phys. Lett.*, 1996, **256**, 454; (*b*) R. E. Stratmann, G. E. Scuseria and M. J. Frisch, *J. Chem. Phys.*, 1998, **109**, 8218; (*c*) M. E. Casida, C. Jamorski, K. C. Casida and D. R. Salahub, *J. Chem. Phys.*, 1998, **108**, 4439.

46 (*a*) V. Barone and M. Cossi, *J. Phys. Chem. A*, 1998, **102**, 1995; (*b*) M. Cossi and V. Barone, *J. Chem. Phys.*, 2001, **115**, 4708; (*c*) M. Cossi, N. Rega, G. Scalmani and V. Barone, *J. Comput. Chem.*, 2003, **24**, 669.

47 S. Leonid, *Chemissian 1.7*. 2005-2010. Available at http://www.chemissian.com.

48 D. A. Zhurko, G. A. Zhurko, *ChemCraft 1.5*; Plimus: San Diego, CA. Available at http://www.chemcraftprog.com.